Tampere University

Alpi Tolvanen

DIAMAGNETIC SUSCEPTIBILITY WITH PATH INTEGRAL MONTE CARLO METHOD

Faculty of Engineering and Natural Sciences
Master of Science
May 2021

ABSTRACT

Alpi Tolvanen: Diamagnetic susceptibility with path integral Monte Carlo method
Master of Science
Tampere University
Computational Physics
May 2021

The diamagnetic susceptibility is an essential magnetic property, as it describes magnetization response of material to an external magnetic field. However, accurate computational data is not available for systems at finite temperatures, because nuclear motion and finite temperature are not well-supported by common *ab initio* simulation methods.

We utilize path integral Monte Carlo method (PIMC), which combines non-relativistic quantum mechanics with statistical mechanics at finite temperatures. PIMC takes exact many-body effects into account, which brings precise simulation of electronic correlation and non-adiabatic nuclei. The accuracy of results is limited by statistical error, which can be controlled with the extent of computation.

In this work, we formulate path integrals and derive an estimator for diamagnetic susceptibility in the limit of zero magnetic field. The estimator is applied in PIMC simulations, and the diamagnetic susceptibility is calculated for $^4\mathrm{He}$, H, H_2, H_2^+, D_2, HD, Ps and Ps_2, where D is a deuterium and Ps is a positronium. The systems are simulated both with nonadiabatic nuclei and with fixed Born–Oppenheimer nuclei. Temperature is varied on range from $300\,\mathrm{K}$ to $3000\,\mathrm{K}$.

The hydrogen atom and the hydrogen molecule express significant nonadiabatic effects in diamagnetic susceptibility, but the helium atom does not. The susceptibility of monatomic systems do not correlate with the temperature, which is expected. The susceptibility of diatomic molecules increases at higher temperatures, which can be explained by a nuclear separation caused by centrifugal forces. The susceptibility of positronium decreases at higher temperatures, which is unexpected.

Obtained PIMC results are compared to $0\,\mathrm{K}$ reference values, because there are nearly no published calculations available at finite temperatures. If the PIMC results are extrapolated at $0\,\mathrm{K}$, they are fairly well in line with the reference values. Overall, PIMC appears to be a good method for calculating exact diamagnetic properties of small molecules.

Keywords: magnetizability, non-Born–Oppenheimer, first principles, imaginary time

TIIVISTELMÄ

Alpi Tolvanen: Diamagneettinen suskeptibiliteetti polkuintegraali–Monte Carlo-menetelmällä
Diplomityö
Tampereen yliopisto
Laskennallinen fysiikka
Toukokuu 2021

Diamagneettinen suskeptibiliteetti on keskeinen magneettinen ominaisuus, sillä se määrittelee materiaalin magneettisen vasteen ulkoisessa magneettikentässä. Kuitenkin, äärellisistä lämpötiloista ei ole tarkkaa laskennallista dataa saatavilla, sillä ytimien liike ja äärellinen lämpötila jätetään huomioimatta useimmissa simulaatiomenetelmissä.

Tässä työssä hyödynnetään polkuintegraali-Monte Carlo-menetelmää (PIMC), joka yhdistää epärelativistisen kvanttimekaniikan ja äärellisen lämpötilan statistisen mekaniikan. PIMC kykenee ottamaan monen kappaleen vuorovaikutukset huomioon eksaktisti, mikä mahdollistaa tarkan simuloinnin sekä elektronikorrelaatiolle että ydinten ei-adibaattisuudelle. PIMC tulosten tarkkuuden määrittää statistinen virheraja, jota voi pienentää laskennallisten resurssien määrällä.

Työssä formuloidaan polkuintegraalit ja johdetaan diamagneettisen suskeptibiliteetin estimaattori nollakenttärajalla. Johdettua estimaattoria sovelletaan PIMC-simulaatioihin, ja diamagneettinen suskeptibiliteetti lasketaan systeemeille $^4\mathrm{He}$, H, H_2, H_2^+, D_2, HD, Ps ja Ps_2, missä D on deuterium ja Ps on positronium. Systeemejä simuloidaan sekä ei-adiabaattisilla ytimillä että kiinteillä Born–Oppenheimer -ytimillä. Lämpötilaa varioidaan välillä 300–$3000\,\mathrm{K}$.

Vetyatomin ja vetymolekyylin diamagneettisissa suskeptibiliteeteissä esiintyy selviä ei-adiabaattista muutoksia, kun taas heliumilla niitä ei esiinny. Monoatomisten systeemien suskeptibiliteetit eivät korreloi lämpötilan kanssa, mikä on odotettua. Diatomisten molekyylien suskeptibiliteetit kohoavat lämpötilan mukaan, minkä voi selittää pyörimisliikkeen kasvattamalla ydinetäisyydellä. Positroniumin suskeptibiliteetti heikkenee korkeammissa lämpötiloissa, mikä on odottamatonta.

Saatuja PIMC tuloksia verrataan $0\,\mathrm{K}$ referenssiarvoihin, sillä äärellisistä lämpötiloista ei ole monia julkaistuja tuloksia saatavilla. Jos PIMC tuloksia ekstrapoloidaan $0\,\mathrm{K}$ lämpötilaan, ovat ne hyvin linjassa referenssiarvojen kanssa. Kaiken kaikkiaan, PIMC vaikuttaa olevan hyvä menetelmä eksaktien diamagneettisten ominaisuuksien laskemisessa pienille molekyyleille.

Avainsanat: magnetoituvuus, ab initio -menetelmä, imaginääriaika

CONTENTS

1 INTRODUCTION

Magnetic susceptibility determines how a material is magnetized in response to an external magnetic field. That is, it determines how much magnetization of material either weakens or strengthens the external magnetic field. In practical terms, if the material weakens the external magnetic field, it repels magnets, and if the material strengthens the external magnetic field, it attracts the magnets. There are two opposing contributions of magnetism, diamagnetism and paramagnetism, and they correspond to the weakening and strengthening effects respectively. The diamagnetism is formed by response of electron motion, and it is present in every material. The paramagnetism is mainly formed by the electron spins, and it is present in materials that have an unpaired number of electrons. Many materials have paired number of electrons, and magnetic moments of the electron spins cancel out rendering the material to be mainly diamagnetic. In this work we focus solely on the diamagnetic contribution, and so diamagnetic susceptibility is also referred with a general term ”susceptibility”.

Magnetic properties of molecules are needed with increasing accuracy. This requires simulation of thermal coupling, nuclear motion and exact many-body effects, which are approximated out in many common simulation methods. The nuclear motion is essential for understanding the effects of temperature, because thermal energy induces vibrations and rotations to molecular bonds. Commonly used simulation methods can only take into account temperature with the approximation that the electron has insignificant mass compared to the nucleus. This approximation is not accurate for light nuclei such as the hydrogen nuclei.

Path Integral Monte Carlo method (PIMC) [1–3] is a lesser-known approach to describe quantum mechanics. PIMC simulates thermal systems by propagating on Feynman path integrals in imaginary-time. PIMC evaluates the path integrals with Monte Carlo sampling, and so the accuracy of results is determined by a statistical error. Within this statistical error, PIMC simulates temperature, nuclear motion and electronic correlation exactly. On the contrary, many quantum simulation methods apply approximations to these effects, which may create a bias that is difficult to estimate [3, 4].

There are not many existing calculations of the diamagnetic susceptibility at the finite temperatures, even though some studies exist [5][6]. There is also no full consensus on nonadiabatic calculations at zero temperature, as varying methods apply different approximations, which produce slightly different results. If PIMC can squeeze the statistical error to small enough, it can help bring settlement with its exact nature.

Temperature-dependent magnetic properties are needed in technologies such as Nuclear Magnetic Resonance (NMR) and Magnetic Resonance Imaging (MRI) [4]. These technologies are commonly calibrated with data from first-principles calculations, because experimental data is not well available [7].

The remainder of this work is organized as follows. In section 2 of this study we introduce theory of real-time path integrals at zero temperature. In section 3 we show how imaginary-time propagation leads to finite temperature properties. In section 4 we derive a general equation for susceptibility, and in section 5 we apply it to derive the diamagnetic susceptibility. In section 6 we give a brief overview of some numerical tools that are used to evaluate imaginary-time path integrals in PIMC. In section 7 we present results for light molecules. Section 8 contains a summary and conclusions. In appendix A we present a brief theory of time-dependent susceptibility, and in appendix B we derive the susceptibility of the hydrogen atom with an infinitely heavy nucleus. In appendix C we provide a link to supplementary information of the simulations.

2 FEYNMAN PATH INTEGRALS

The quantum mechanics cannot be derived from the classical mechanics, and thus, different postulates are required to describe it. A conventional formulation of the quantum mechanics is tightly linked to the Schrödinger equation, but in this work we take a different approach by focusing on an alternative formulation known as Feynman's path integrals [8]. Where the Schrödinger equation takes so-called *Hamiltonian* as a starting point, the path integrals take so-called *Lagrangian*. The path integrals can be derived from the Schrödinger equation, and vice versa.

A general idea behind the path integral formulation is that it affiliates a complex number with any arbitrary trajectory that corresponds to a particle moving from one point to another. This complex number is then summed over all possible trajectories between the two points, no matter how arbitrary they are. The squared norm of the sum represents the probability that such movement is observed.

In this chapter we follow Feynman's approach [8], which intuitively introduces the path integrals from the double-slit experiment. We present two postulates of the path integral formalism, and then we loosely build the quantum mechanical equations on top them. Also, we establish a connection between the path integrals and the wave function.

2.1 Double-slit experiment

The double-slit experiment is a well-known demonstration that brings up wave-like nature of particles. Figure 2.1 shows a basic configuration of the double-slit experiment. A particle source at point A shoots particles towards a barrier with two slits. The particles pass the slits and form an interference pattern on a detector screen D.

The interference pattern can be explained with the use of *probability amplitudes*. The probability amplitude is a complex-valued function which represents information of the phase and amplitude. Let the probability amplitude $\phi_{a,b} \in \mathbb{C}$ correspond to the movement of a particle from point a to point b. Squaring the norm of the amplitude gives the probability of observing such movement, that is,

$$P_{a,b} = |\phi_{a,b}|^2. \tag{2.1}$$

Consider first that only the slit B is open in figure 2.1. Then, the particle trajectory passes through points $A \to B \to D$, and the corresponding probability amplitude is $\phi_{A,B,D}$. This

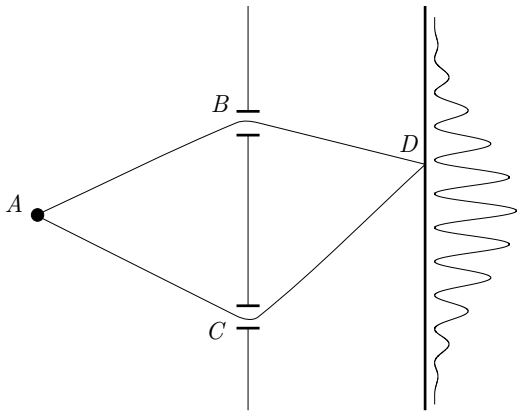

Figure 2.1. *Double-slit experiment containing a particle source A, a barrier screen with two slits B and C, and a point D on a detector screen. The particle passes through the slits and forms an interference pattern. Image from [9].*

probability amplitude can be split in two parts

$$\phi_{A,B,D} = \phi_{A,B}\phi_{B,D}. \tag{2.2}$$

This may be a familiar property from wave mechanics: phases are summed and amplitudes multiplied. That is, if A is a scalar amplitude and θ is the phase, then the multiplication can be expressed as $\left(A_1 e^{\mathrm{i}\theta_1}\right)\left(A_2 e^{\mathrm{i}\theta_2}\right) = A_1 A_2 e^{\mathrm{i}(\theta_1+\theta_2)}$.

When both of the slits B and C are open, the wave passes simultaneously through both of them, forming an interference pattern on the detection screen. The observation probability is not a sum of two separately observed probabilities

$$P_{A,D} \neq P_{A,B,D} + P_{A,C,D} = |\phi_{A,B,D}|^2 + |\phi_{A,C,D}|^2. \tag{2.3}$$

Instead, the probability amplitudes must be summed first, and the square must be taken after [8]

$$P_{A,D} = |\phi_{A,B,D} + \phi_{A,C,D}|^2 = |\phi_{A,D}|^2. \tag{2.4}$$

However, if the location of the particle was observed at either slit, then the interference would not take place. This is a fundamental aspect in Feynman's original formulation [10]: The total observation probability depends on whether intermediate probabilities have well-defined values or not. Observing the particle at the slit has a well-defined probability, but not observing the particle has an undefined probability.

The double-slit experiment can be generalized to include more than two slits. If the barrier screen has I slits, then the total probability amplitude is just a sum over all trajectories

$$\phi_{A,D} = \sum_{i}^{I} \phi_{A,i,D}. \tag{2.5}$$

Continuing with generalizations, there can be more barrier screens than just one. The total probability amplitude is a sum over all different combinations in which the particle can pass through all the slits. For example, if there were two screens with I and J slits each, then the total probability amplitude would be

$$\phi_{A,D} = \sum_{i}^{I} \sum_{j}^{J} \phi_{A,i,j,D}. \tag{2.6}$$

The situation with $I = 3$ and $J = 2$ is illustrated in figure 2.2.

The number of barrier screens and the number of slits can be increased arbitrarily. The limit at infinity exists [8, p. 33], and it corresponds to a free particle with no slits at all. The summation of amplitudes over all possible trajectories can be compared to Huygens–Fresnel principle in the classical wave mechanics[10, p. 19], which states that every point of a wavefront is itself a source of spherical wavelets.

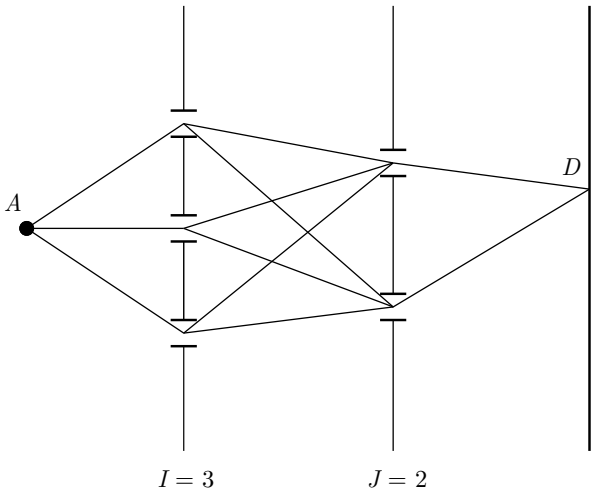

Figure 2.2. *Generalized slit experiment with two barrier screen. The total probability amplitude is a sum over all different combinations of trajectories.*

2.2 Kernel for a single particle

Let there be two events $a = (\boldsymbol{r}_a,\ t_a)$ and $b = (\boldsymbol{r}_b,\ t_b)$, so that $t_a < t_b$. So far, explicit information of time has been left out from the total probability amplitude notation $\phi_{\boldsymbol{r}_a,\boldsymbol{r}_b}$. When the information of time is included in $\phi_{\boldsymbol{r}_a,\boldsymbol{r}_b}$, it is called a *kernel*. This work assumes time-independent systems, and so the time difference $t_b - t_a$ is enough to describe the time-dependence of the kernel. Let $\boldsymbol{r}(t)$ be an arbitrary trajectory of a particle such that $\boldsymbol{r}(t_a) = \boldsymbol{r}_a$ and $\boldsymbol{r}(t_b) = \boldsymbol{r}_b$. Let $\phi[\boldsymbol{r}(t)]$ be a partial probability amplitude associated with the trajectory. The notation $\phi[\cdot]$ denotes a functional, meaning that it reduces the function $\boldsymbol{r}(t)$ into a scalar number. The kernel is

$$K(\boldsymbol{r}_a, \boldsymbol{r}_b, t_b - t_a) = \sum_{\text{all trajectories}} \phi[\boldsymbol{r}(t)] \tag{2.7}$$

$$\equiv \int_{\boldsymbol{r}(t_a)=\boldsymbol{r}_a}^{\boldsymbol{r}(t_b)=\boldsymbol{r}_b} \mathcal{D}\boldsymbol{r}(t)\ \phi[\boldsymbol{r}(t)], \tag{2.8}$$

where $\mathcal{D}\boldsymbol{r}(t)$ denotes a functional integral. Because the kernel is the probability amplitude, the probability of the particle moving from event a to event b is given by equation 2.1

$$P_{a,b} = |K(\boldsymbol{r}_a, \boldsymbol{r}_b, t_b - t_a)|^2. \tag{2.9}$$

The equations 2.8 and 2.9 form Feynman's first postulate of the quantum mechanics [10]. The second postulate is that the probability amplitude of the trajectory is

$$\phi[\boldsymbol{r}(t)] = \mathcal{A}\ e^{\frac{\mathrm{i}}{\hbar} S[\boldsymbol{r}(t)]}, \tag{2.10}$$

where $\mathcal{A}$ is a normalization constant, i is an imaginary unit, $\hbar$ is a reduced Planks constant, and S is a classical *action*. The classical action is

$$S[\boldsymbol{r}(t)] = \int_{t_a}^{t_b} \mathrm{d}t\, L\left(\dot{\boldsymbol{r}}(t), \boldsymbol{r}(t)\right), \tag{2.11}$$

where L is the classical *Lagrangian* and $\dot{\boldsymbol{r}}(t) = \frac{\mathrm{d}\boldsymbol{r}(t)}{\mathrm{d}t}$ is velocity. The classical Lagrangian is

$$L\left(\dot{\boldsymbol{r}}, \boldsymbol{r}\right) = \underbrace{\frac{m}{2}\dot{\boldsymbol{r}}^2}_{\mathcal{K}(\dot{\boldsymbol{r}})} - V\left(\boldsymbol{r}\right), \tag{2.12}$$

where m is the mass of the particle, $\mathcal{K}$ is the kinetic energy and V is the potential energy.

Equations 2.2 and 2.5 make it possible to combine two kernels into one kernel with a longer time difference. If the first kernel propagates time $t_a \to t_b$ and the second propagates $t_b \to t_c$, then the combined kernel propagates $t_a \to t_c$. This is

$$K(\boldsymbol{r}_a, \boldsymbol{r}_c, t_c - t_a) = \int_{-\infty}^{\infty} \mathrm{d}\boldsymbol{r}_b\, K(\boldsymbol{r}_a, \boldsymbol{r}_b, t_b - t_a) K(\boldsymbol{r}_b, \boldsymbol{r}_c, t_c - t_b), \tag{2.13}$$

where $t_a < t_b < t_c$, and $\mathrm{d}\boldsymbol{r}_b$ denotes a multidimensional integration over the coordinate space.

2.3 Kernel for multiple particles

Generalization for multiple particles is straightforward. Let there be N distinguishable particles whose coordinates are denoted with

$$R = [\boldsymbol{r}_1, \boldsymbol{r}_2, \dots \boldsymbol{r}_N]^T \tag{2.14}$$

$$= [r_{11}, \dots r_{1d}, r_{21} \dots r_{Nd}]^T, \tag{2.15}$$

where d is the number of dimensions. In this work $d = 3$.

The kernel, the action, and the Lagrangian are respectively

$$K(R_a, R_b, t_b - t_a) = \int_{R(t_a)=R_a}^{R(t_b)=R_b} \mathcal{D}R(t)\, \mathcal{A} e^{\frac{\mathrm{i}}{\hbar} S[R(t)]} \tag{2.16}$$

$$S[R(t)] = \int_{t_a}^{t_b} \mathrm{d}t\, L\left(\dot{R}(t), R(t)\right) \tag{2.17}$$

$$L\left(\dot{R}, R\right) = \sum_n^N \frac{m_n}{2} \dot{\boldsymbol{r}}_n{}^2 - V(R). \tag{2.18}$$

The potential term V depends on the particular system, and in this work it is the Coulomb potential of charged particles

$$V(R) = \sum_{n'>n}^{N} \frac{1}{4\pi\varepsilon_0} \frac{q_n q_{n'}}{|\boldsymbol{r}_n - \boldsymbol{r}_{n'}|}, \tag{2.19}$$

where ε_0 is a vacuum permittivity and q is a charge. Slight inconveniences will later emerge from the fact that the Coulomb potential is not bounded from below.

The case of indistinguishable particles is briefly mentioned in the section 6.6.

2.4 Discretization at the limit of short timestep

The functional integral 2.16 can be transformed into an alternative representation by dividing it into short time steps. The time range $t_b - t_a$ can be divided into M time steps such that $M\Delta t = t_b - t_a$. If a time step Δt is differentially short, then the kernel $K(\Delta t)$ has an analytical expression. The equation 2.13 can be applied M times, which in the

limit of $M \to \infty$ and $\Delta t \to 0$ yields

$$
\begin{aligned}
&K(R_a, R_b, t_b - t_a) \\
&\quad = \lim_{M\to\infty} \left(\int \cdots \int \mathrm{d}R_1 \mathrm{d}R_2 \cdots \mathrm{d}R_{M-1}\; K(R_0, R_1, \Delta t) \cdots K(R_{M-1}, R_M, \Delta t) \right) \qquad (2.20) \\
&\quad = \lim_{M\to\infty} \left(\int \cdots \int \prod_{m=1}^{M-1} \mathrm{d}R_m \prod_{m=0}^{M-1} K(R_m, R_{m+1}, \Delta t) \right), \qquad (2.21)
\end{aligned}
$$

where labels R_0, R_M correspond to points R_a, R_b.

The next task is to find an analytical formula for the kernel $K(R_m, R_{m+1}, \Delta t)$. If the time difference Δt is differentially short, then all trajectories cancel each other out except for the classical trajectory $R_{\mathrm{cl}}(t)$. The kernel can be then calculated with

$$K(R_a, R_b, \Delta t) = A e^{\frac{\mathrm{i}}{\hbar} S[R_{\mathrm{cl}}(t)]}, \qquad (2.22)$$

where A is a normalization constant. Here we give a brief reasoning why the non-classical trajectories are cancelled in the functional integration. The classical path $R_{\mathrm{cl}}(t)$ minimizes the action S, and the paths near $R_{\mathrm{cl}}(t)$ evaluate almost the same values of S. This creates a constructive interference in the summation of the terms $e^{\frac{\mathrm{i}}{\hbar} S}$. However, if the paths are far away from $R_{\mathrm{cl}}(t)$, then small path deviations vary S rapidly, and the phase of $e^{\frac{\mathrm{i}}{\hbar} S}$ also varies rapidly, which makes the paths mostly cancel each other out in the summation. See Feynman's work [8, p. 30] for a more detailed explanation. As a brief side note, scaling $\hbar \to 0$ would also increase the variance of $\frac{\mathrm{i}}{\hbar} S$ resulting cancellation of the non-classical paths. That is, scaling $\hbar \to 0$ yields the classical mechanics.

It is worth noting that equations 2.21 and 2.22 do not directly apply for potentials that are unbounded from below, no matter how short Δt is. A workaround for the Coulomb potentials is presented in references [2][11, p. 918][12, p. 81].

In the limit of differentially short time step, the classical trajectory corresponds to particles moving in straight lines with constant velocities [8, p. 33]. The Lagrangian is constant on a short trajectory, and the action integral 2.17 can be written to depend only on its end points with

$$S[R_{\mathrm{cl}}(t)] = S\left(R_a, R_b, \Delta t\right). \qquad (2.23)$$

The discretized kernel 2.21 is valid with either of the following two actions [10, p. 15]

$$
\begin{aligned}
S\left(R_a, R_b, \Delta t\right) &= \Delta t\; L\left(\frac{R_b - R_a}{\Delta t}, \frac{R_a + R_b}{2}\right) \qquad (2.24) \\
S\left(R_a, R_b, \Delta t\right) &= \Delta t\; \frac{1}{2}\left(L\left(\frac{R_b - R_a}{\Delta t}, R_a\right) + L\left(\frac{R_b - R_a}{\Delta t}, R_b\right)\right). \qquad (2.25)
\end{aligned}
$$

If the Lagrangian does not depend linearly on velocity, that is, there is no magnetic field,

then following action is also valid

$$S\left(R_a, R_b, \Delta t\right) = \Delta t \; L\left(\frac{R_b - R_a}{\Delta t}, R_a\right). \tag{2.26}$$

There is some freedom in evaluating the potential term $V(R)$ in the Lagrangian, so that the kernel 2.21 still remains effectively unchanged. The potential term can be evaluated anywhere between endpoints R_a and R_b, or it can be calculated as any linear combination of $V(R_a)$ and $V(R_b)$ [13].

The normalization constant in equation 2.22 is [10, p. 18]

$$A = \prod_n^N \left(\frac{m_n}{2\pi \mathrm{i}\hbar\Delta t}\right)^{\frac{d}{2}}. \tag{2.27}$$

Now the kernel is fully described. It is

$$K(R_a, R_b, t_b - t_a) = \lim_{M\to\infty}\left(\int\cdots\int \prod_{m=1}^{M-1} \mathrm{d}R_m \prod_{m=0}^{M-1} A e^{\frac{\mathrm{i}}{\hbar}S(R_m, R_{m+1}, \Delta t)}\right), \tag{2.28}$$

where $R_0 = R_a$ and $R_M = R_b$.

2.5 The kernel of free particles

If there is no potential, the kernel corresponds to free particles, which has an analytical solution [8, pp. 42, 66]

$$K(R_a, R_b, t_b - t_a) = A \exp\left\{\frac{\mathrm{i}}{\hbar}\sum_n \frac{m_n\left(\boldsymbol{r}_b - \boldsymbol{r}_a\right)^2}{2\left(t_b - t_a\right)}\right\}. \tag{2.29}$$

This solution holds for any time range $t_b - t_a$.

2.6 External magnetic field

This section shows how magnetic field is included into the Lagrangian of classical particles. Equations of magnetism are presented with the SI convention, which does contain some differences to equations utilizing Gaussian convention.

2.6.1 Magnetic Lagrangian

Let there be a spinless charged particle affected by a magnetic field. It has a classical Lagrangian [11, p. 179] [8, p. 189]

$$L(\dot{\boldsymbol{r}}, \boldsymbol{r}) = \underbrace{\frac{m}{2}\dot{\boldsymbol{r}}^2 - V(\boldsymbol{r})}_{L_0(\dot{\boldsymbol{r}}, \boldsymbol{r})} + \underbrace{q\boldsymbol{A}(\boldsymbol{r})\cdot\dot{\boldsymbol{r}}}_{L_M(\dot{\boldsymbol{r}}, \boldsymbol{r})}, \tag{2.30}$$

where $\boldsymbol{A}$ is a magnetic vector potential, L_0 is a Lagrangian without magnetic interaction, and L_M is a magnetic interaction term. Assuming a homogeneous magnetic field $\boldsymbol{B}$, the vector potential can be chosen to be

$$\boldsymbol{A}(\boldsymbol{r}) = \frac{1}{2}\boldsymbol{B} \times \boldsymbol{r}, \tag{2.31}$$

with which the magnetic interaction becomes

$$L_M(\dot{\boldsymbol{r}}, \boldsymbol{r}) = \frac{q}{2}(\boldsymbol{B} \times \boldsymbol{r}) \cdot \dot{\boldsymbol{r}}. \tag{2.32}$$

Using a vector identity

$$(\boldsymbol{a} \times \boldsymbol{b}) \cdot \boldsymbol{c} = (\boldsymbol{b} \times \boldsymbol{c}) \cdot \boldsymbol{a}, \tag{2.33}$$

it becomes

$$\begin{aligned} L_M(\dot{\boldsymbol{r}}, \boldsymbol{r}) &= \frac{q}{2}(\boldsymbol{r} \times \dot{\boldsymbol{r}}) \cdot \boldsymbol{B} && (2.34)\\ &= \frac{q}{2m}(\boldsymbol{r} \times \boldsymbol{p}) \cdot \boldsymbol{B} && (2.35)\\ &= \boldsymbol{m} \cdot \boldsymbol{B}, && (2.36) \end{aligned}$$

where $\boldsymbol{p} = m\dot{\boldsymbol{r}}$ is the momentum, and $\boldsymbol{m} = \frac{q}{2m}\boldsymbol{r} \times \boldsymbol{p}$ is the magnetic dipole moment.

2.6.2 Many-body Lagrangian

Let there be multiple spinless charged particles in a magnetic field, for which the Lagrangian is [11, p. 179][14]

$$L\left(\dot{R}, R\right) = \underbrace{\sum_n^N \frac{m_n}{2}\dot{\boldsymbol{r}}_n^2 - V(R)}_{L_0\left(\dot{R},R\right)} + \underbrace{\sum_n^N q_n \boldsymbol{A}(\boldsymbol{r}_n) \cdot \dot{\boldsymbol{r}}_n}_{L_M\left(\dot{R},R\right)}. \tag{2.37}$$

Assuming no magnetic interaction between the particles, the vector potential is given by equation 2.31. The equation 2.37 can be written

$$\begin{aligned} L\left(\dot{R}, R\right) &= L_0\left(\dot{R}, R\right) + \left(\sum_n^N \frac{q_n}{2}(\boldsymbol{r}_n \times \dot{\boldsymbol{r}}_n)\right) \cdot \boldsymbol{B} && (2.38)\\ &= L_0\left(\dot{R}, R\right) + \boldsymbol{m}\left(\dot{R}, R\right) \cdot \boldsymbol{B}, && (2.39) \end{aligned}$$

where $\boldsymbol{m}$ is the total magnetic dipole moment.

The magnetic interaction between the particles is neglected because it is fundamentally a relativistic effect. Fortunately, the relativistic effects are marginal on light molecules. For example, relativistic energy of the hydrogen molecule shows up only in fifth decimal [15].

If some basic magnetic interactions were required to be taken into account, they can be included as a relativistic correction, from which the *Darwin Lagrangian* [14] is a good example.

2.6.3 Action

Combining equation 2.30 with 2.25 gives short time step action for the particle in the magnetic field [10, p. 15][13]

$$S(\boldsymbol{r}_a, \boldsymbol{r}_b, \Delta t) = \Delta t \frac{1}{2}\left(L\left(\frac{\boldsymbol{r}_b - \boldsymbol{r}_a}{\Delta t}, \boldsymbol{r}_a\right) + L\left(\frac{\boldsymbol{r}_b - \boldsymbol{r}_a}{\Delta t}, \boldsymbol{r}_b\right)\right) \tag{2.40}$$

$$= \Delta t\left(\frac{m}{2}\left(\frac{\boldsymbol{r}_b - \boldsymbol{r}_a}{\Delta t}\right)^2 - \frac{V(\boldsymbol{r}_a) + V(\boldsymbol{r}_b)}{2} + q\frac{\boldsymbol{A}(\boldsymbol{r}_a) + \boldsymbol{A}(\boldsymbol{r}_b)}{2} \cdot \frac{\boldsymbol{r}_b - \boldsymbol{r}_a}{\Delta t}\right). \tag{2.41}$$

This results in a kernel, whose error is known to scale with $\Delta t^{\frac{3}{2}}$, that is

$$K(\boldsymbol{r}_a, \boldsymbol{r}_b, \Delta t) = Ae^{\frac{\mathrm{i}}{\hbar}S(\boldsymbol{r}_a, \boldsymbol{r}_b, \Delta t)} + \mathrm{O}(\Delta t^{\frac{3}{2}}). \tag{2.42}$$

In contrast, if there is no magnetic field, the action 2.26 poses an error that scales to Δt^2 [13]. The normalization constant A does not depend on the magnetic field, and it is the same as in equation 2.27.

2.6.4 Free particle in a magnetic field

There exists an analytical solution for the kernel of a free particle in a constant magnetic field B in the z-direction. The kernel is [8, p. 64] [16]

$$K(\boldsymbol{r}_a, \boldsymbol{r}_b, t_b - t_a) = \left(\frac{m}{2\pi \mathrm{i}\hbar(t_b - t_a)}\right)^{\frac{3}{2}} \left(\frac{\frac{\omega(t_b - t_a)}{2}}{\sin\left(\frac{\omega(t_b - t_a)}{2}\right)}\right) \exp\left\{\frac{\mathrm{i}m}{2\hbar}\left[\frac{(z_b - z_a)^2}{t_b - t_a}\right.\right. \tag{2.43}$$

$$\left.\left. + \left(\frac{\frac{\omega}{2}}{\tan\left(\frac{\omega(t_b - t_a)}{2}\right)}\right)\left((x_b - x_a)^2 + (y_b - y_a)^2\right) + \omega\left(x_a y_b - x_b y_a\right)\right]\right\} \tag{2.44}$$

where $\omega = \frac{eB}{m}$ is cyclotron frequency. This kernel is valid for any time difference $t_b - t_a$.

2.7 Wave function

Because the path integral formulation is less well known than Schrödinger wave mechanics, their connection is important to clarify. In this section we show how these formulations can be represented with each other.

In previous sections we have shown how the kernel determines the probability amplitude from event (R_a, t_a) to event (R_b, t_b). However, the point of interest is not always (R_a, t_a),

but rather the evolution of the probability amplitude. If the starting point is dropped out of the kernel, it is known better as the *wave function* [8, p. 57]

$$\psi(R_b, t_b) = K(\,\cdot\,,\ R_b,\ t_b - \cdot\,). \tag{2.45}$$

Equation 2.9 gives a probability density of finding the system in a configuration R, which is

$$P(R) = |\psi(R)|^2 = \psi^*(R)\psi(R), \tag{2.46}$$

where * denotes the complex conjugate. Here the time argument has been dropped out of the wave function, because the system is assumed to be time-independent, which results trivial time-dependence of ψ. The wave function describes a *state* of the system, which defines a probability distribution for physical quantities. Let us consider an observable O, which is a physical quantity associated with a Hermitian operator $\hat{O}$. The expectation value of $\hat{O}$ is

$$\left\langle \hat{O} \right\rangle = \int \mathrm{d}R\ \psi^*(R)\hat{O}\psi(R) \equiv\ \langle\psi|\hat{O}|\psi\rangle\,, \tag{2.47}$$

where $\langle\cdot|\cdot|\cdot\rangle$ is braket notation.

The evolution of the state is described by the Schrödinger equation

$$\mathrm{i}\hbar\frac{\partial\psi(R,t)}{\partial t} = \left(\sum_n^N \frac{1}{2m_n}\hat{\boldsymbol{p}}_n^2 + V(R)\right)\psi(R,t) \tag{2.48}$$

$$= \hat{H}\psi(R,t) \tag{2.49}$$

where $\hat{\boldsymbol{p}}_n = -\mathrm{i}\hbar\nabla_n$ is the momentum operator and $\hat{H}$ is the Hamiltonian operator. If the system is time-independent, then the time-dependence of the solution $\psi(R,t)$ can be separated, and the resulting time-independent wave function $\psi(R)$ can be decomposed into an orthonormal set of *energy eigenstates* with $\psi = \sum_i c_i\phi_i$, where $c_i \in \mathbb{C}$, and the eigenstates ϕ_i fulfill $\hat{H}\phi_i = E_i\phi_i$. The terms $|c_i|^2$ correspond to a probability that the system is measured with an energy E_i. It is said that $\hat{H}$ is *diagonal* to ϕ_i.

2.7.1 Propagator

Equation 2.13 shows that a kernel moves another kernel in time. This is why the kernel is called the *propagator* of the wave function, that is

$$\psi(R_b, t_b) = \int \mathrm{d}R_a K(R_a, R_b, t_b - t_a)\psi(R_a, t_a). \tag{2.50}$$

The propagation can be also expressed as a time evolution operator U [10]

$$\psi(R_b, t_b) = \underbrace{e^{-\frac{\mathrm{i}}{\hbar}(t_b - t_a)\hat{H}}}_{U(t_b - t_a)} \psi(R_a, t_a). \tag{2.51}$$

The propagated wave function can be written as

$$\begin{aligned}
\psi(R_b, t_b) &= \langle R_b | \psi(t_b) \rangle && (2.52)\\
&= \langle R_b | e^{-\frac{\mathrm{i}}{\hbar}(t_b - t_a)\hat{H}} | \psi(t_a) \rangle && (2.53)\\
&= \left\langle R_b \middle| e^{-\frac{\mathrm{i}}{\hbar}(t_b - t_a)\hat{H}} \left(\int \mathrm{d}R_a \ |R_a\rangle\langle R_a| \right) \psi(t_a) \right\rangle && (2.54)\\
&= \int \mathrm{d}R_a \ \underbrace{\langle R_b | e^{-\frac{\mathrm{i}}{\hbar}(t_b - t_a)\hat{H}} | R_a \rangle}_{K} \psi(R_a, t_a), && (2.55)
\end{aligned}$$

which gives an alternative expression for the kernel as

$$K(R_a, R_b, t_b - t_a) = \langle R_b | e^{-\frac{\mathrm{i}}{\hbar}(t_b - t_a)\hat{H}} | R_a \rangle . \tag{2.56}$$

In the position basis, the representation of the state $|R\rangle$ is a Dirac delta function, that is, $\langle R_a | R_b \rangle = \delta(R_a, R_b)$ and $\langle R | \psi(t) \rangle = \psi(R, t)$.

2.7.2 Transition amplitude

As is previously stated, the kernel determines the probability amplitude from one point to another. A *transition amplitude* is a generalization that determines the probability amplitude from one state to another. The transition amplitude from state $\psi(t_a)$ to state $\phi(t_b)$ is [8, p.165]

$$\begin{aligned}
&\left\langle \phi \middle| e^{-\frac{\mathrm{i}}{\hbar}(t_b - t_a)\hat{H}} \middle| \psi \right\rangle && (2.57)\\
&= \int\int \mathrm{d}R_a \mathrm{d}R_b \ \phi^*(R_b, t_b) K(R_a, R_b, t_b - t_a) \psi(R_a, t_a) && (2.58)\\
&= \int\int \mathrm{d}R_a \mathrm{d}R_b \ \phi^*(R_b, t_b) \left(\int_{R(t_a)=R_a}^{R(t_b)=R_b} \mathcal{D}R(t) \ \mathcal{A} e^{\frac{\mathrm{i}}{\hbar} S[R(t)]} \right) \psi(R_a, t_a) && (2.59)\\
&\equiv \left\langle \phi(t_b) \middle| 1 \middle| \psi(t_a) \right\rangle_S , && (2.60)
\end{aligned}$$

where equation 2.16 is inserted on the line 2.59, and the braket-like notation 2.60 follows the reference [8, p.165]. Note that 2.60 is not a conventional braket notation, because the "1" is a placeholder for a functional, which multiplies each individual path in the functional integration. Placing a functional $O\left[R(t)\right]$ in the transition amplitude reads

$$\left\langle \phi(t_b) \middle| O \middle| \psi(t_a) \right\rangle = \int\int \mathrm{d}R_a \mathrm{d}R_b \int_{R(t_a)=R_a}^{R(t_b)=R_b} \mathcal{D}R(t) \ O\left[R(t)\right] \mathcal{A} e^{\frac{\mathrm{i}}{\hbar} S[R(t)]} \phi^*(R_b, t_b) \psi(R_a, t_a). \tag{2.61}$$

It is clear that a kernel expressed as the transition amplitude is

$$K(R_a, R_b, t_b - t_a) = \langle R_b(t_b)|1|R_a(t_a)\rangle \,. \tag{2.62}$$

3 QUANTUM STATISTICAL MECHANICS AND IMAGINARY TIME

Quantum statistical mechanics studies quantum systems in the thermal equilibrium. The effects of finite temperature appear most prominently with the multiatomic molecules, because the thermal energy induces motion to the nuclear bonds by activating rotational and vibrational states. At the room temperature this affects the total energy on the order of percent, and therefore the ground state calculation at zero temperature may not be accurate enough in many realistic situations.

In previous chapter we considered cases where the system is described by a pure quantum state, such as the ground state at zero temperature. However, at finite temperatures there are multiple possible states, where the exact state of the system is not known, but the probability distribution of the states is known. In quantum statistical mechanics the distributions of the states is studied rather than the particular states.

In this section we describe the thermal distribution of the quantum states, and then we express it with the imaginary time path integrals. Last, we use the path integrals to derive the thermal expectation value of an observable.

3.1 Partition function and density matrix

Given unlimited time, practically all systems settle to the thermal equilibrium, which is associated with some temperature T. A single state in the equilibrium has a probability

$$P_i = \frac{1}{Z} e^{-\beta E_i}, \tag{3.1}$$

where Z is a *partition function*, E_i is an energy of state and $\beta = \frac{1}{k_B T}$ is an inverse temperature. Here k_B is the Boltzmann's constant. The partition function acts as a normalization constant, and it is

$$Z = \sum_i e^{-\beta E_i}. \tag{3.2}$$

If O is some measurable quantity of the system, equation 3.1 gives the expectation value as

$$\langle O \rangle = \frac{1}{Z} \sum_i O_i e^{-\beta E_i}. \tag{3.3}$$

Because the partition function Z depends on the properties of the system, all quantities of the classical thermodynamics can be derived from it [8, p. 272]. These quantities include internal energy, entropy, and susceptibility, for example. There are other quantities that cannot be determined directly from the partition function, such as the probability density $P(R)$. However, the probability density can be expressed by combining equation 3.3 with equation 2.46 as [8, p. 272]

$$P(R) = \frac{1}{Z} \sum_i \left(\phi_i^*(R)\phi_i(R)\right) e^{-\beta E_i} \tag{3.4}$$

$$= \frac{1}{Z} \rho\left(R, R, \beta\right), \tag{3.5}$$

where ϕ_i is an energy eigenstate and

$$\rho\left(R_a, R_b, \beta\right) = \sum_i \phi_i(R_a)\phi_i^*(R_b) e^{-\beta E_i} \tag{3.6}$$

is the thermal *density matrix*. The density matrix is a quantum mechanical generalization of the partition function, and it is capable of defining all physical quantities of the system. The relation between the two is

$$Z = \int \mathrm{d}R \, \rho\left(R, R, \beta\right). \tag{3.7}$$

The density matrix $\rho\left(R_a, R_b, \beta\right)$ determines the probability that a system moves from state R_a to state R_b in inverse temperature β. Even though this work takes the probability distribution from the thermal equilibrium, it is not required in the general definition of the density matrix.

Important distinction must be made between the density matrix and an entangled quantum state. The density matrix is a set of pure quantum states, where each state is associated with a classical probability. On the other hand, the entangled state is itself a pure quantum state, and while it is a linear combination of other pure states, the state coefficients are complex-valued.

The density matrix is usually defined more conveniently as

$$\rho\left(R_a, R_b, \beta\right) = \langle R_b | e^{-\beta \hat{H}} | R_a \rangle \tag{3.8}$$

$$= \langle R_b | \hat{\rho}_\beta | R_a \rangle, \tag{3.9}$$

where $\hat{\rho}_\beta$ is the *density operator*. The equation 3.6 can be constructed with

$$\langle R_b|e^{-\beta\hat{H}}|R_a\rangle = \sum_{i,j} \langle R_b|\phi_i\rangle \, \langle\phi_i|e^{-\beta\hat{H}}|\phi_j\rangle \, \langle\phi_j|R_a\rangle \tag{3.10}$$

$$= \sum_{i,j} \phi_i(R_b) \, \langle\phi_i|e^{-\beta E_j}|\phi_j\rangle \, \phi_j^*(R_a) \tag{3.11}$$

$$= \sum_i \phi_i(R_b)\phi_i^*(R_a)e^{-\beta E_i}, \tag{3.12}$$

where equation 3.11 applies an operator exponential series, and equation 3.12 utilizes orthonormality of eigenstates.

The density function 3.7 can be presented with a *trace* of $\hat{\rho}_\beta$

$$Z = \int \mathrm{d}R \, \langle R|\hat{\rho}_\beta|R\rangle \tag{3.13}$$

$$\equiv \mathrm{Tr}\left[\hat{\rho}_\beta\right]. \tag{3.14}$$

An expectation value of the observable $\hat{O}$ in the thermal equilibrium is

$$\left\langle \hat{O} \right\rangle = \frac{1}{Z} \int \mathrm{d}R \, \langle R|e^{-\beta\hat{H}}\hat{O}|R\rangle \tag{3.15}$$

$$= \frac{1}{Z} \, \mathrm{Tr}\left[\hat{\rho}_\beta \hat{O}\right]. \tag{3.16}$$

This expectation value is clearly apparent for diagonal operators if equations 3.10–3.12 are utilized.

3.2 Imaginary time

One of the main benefits of the path integral formalism arises in the quantum statistical mechanics. Notice how similar the kernel 2.56 is to the density matrix 3.8. If the term $\frac{\mathrm{i}}{\hbar}(t_b - t_a)$ is replaced with β, then the kernel becomes the density matrix. Luckily, such replacement can be performed, because the kernel has convenient analytic properties in the complex plane. This is known as the Wick rotation. The kernel that propagates in "the imaginary time" $t_b - t_a = -\mathrm{i}\hbar\beta$ is equal to the density matrix in the inverse temperature β. That is,

$$\rho\left(R_a, R_b, \beta\right) = K(R_a, R_b, -\mathrm{i}\hbar\beta). \tag{3.17}$$

The imaginary time is denoted with $\tau \in \mathbb{R}_+$ so that $t = -\mathrm{i}\hbar\tau$, and an imaginary time trajectory is denoted with $R'(\tau) = R(-\mathrm{i}\hbar\tau)$. Direct substitution of the imaginary time to kernel 2.16 gives [17]

$$\rho\left(R_a, R_b, \beta\right) = \int_{R'(0)=R_a}^{R'(\beta)=R_b} \mathcal{D}R'(\tau) \, \mathcal{A}e^{-S'[R'(\tau)]}, \tag{3.18}$$

where $S' = \mathrm{i}\hbar S$ is the imaginary time action

$$S'[R'(\tau)] = -\int_0^\beta \mathrm{d}\tau\, L\left(\frac{1}{-\mathrm{i}\hbar}\frac{\mathrm{d}R'(\tau)}{\mathrm{d}\tau}, R'(\tau)\right) \tag{3.19}$$

$$= \int_0^\beta \mathrm{d}\tau \left(\sum_n^N \frac{m_n}{2\hbar^2}\left(\frac{\mathrm{d}\boldsymbol{r}_n}{\mathrm{d}\tau}\right)^2 + \sum_{n'>n}^N V\left(\boldsymbol{r}_n, \boldsymbol{r}_{n'}\right)\right). \tag{3.20}$$

The symbols ρ, R' and S' are introduced to conceal the imaginary time constant $-\mathrm{i}\hbar$ in terms K, R and $\frac{\mathrm{i}}{\hbar}S$ respectively. Similarly, plugging the imaginary time in the discretized kernel 2.28 enables writing the density matrix as

$$\rho\left(R_a, R_b, \beta\right) = \lim_{M\to\infty}\left(\int\cdots\int \prod_{m=1}^{M-1}\mathrm{d}R_m \prod_{m=0}^{M-1}\rho\left(R_m, R_{m+1}, \Delta\tau\right)\right), \tag{3.21}$$

where $\Delta\tau = \frac{\beta}{M}$, $R_0 = R_a$, $R_M = R_b$, and the high temperature density matrix is

$$\rho\left(R_a, R_b, \Delta\tau\right) = Ae^{-S'(R_a, R_b, \Delta\tau)}. \tag{3.22}$$

Using the normalization constant 2.27, the action 2.22, and the zero-field Lagrangian 2.26, the high temperature density matrix is

$$\rho\left(R_a, R_b, \Delta\tau\right) = \left(\prod_n^N \left(\frac{m_n}{2\pi\hbar^2\Delta\tau}\right)^{\frac{d}{2}}\right)\exp\left\{-\Delta\tau\,\left(\sum_n^N \frac{m_n}{2\hbar^2}\frac{\left(\boldsymbol{r}_{n,b} - \boldsymbol{r}_{n,a}\right)^2}{\Delta\tau^2} + \sum_{n'>n}^N V\left(\boldsymbol{r}_{n,a}, \boldsymbol{r}_{n',a}\right)\right)\right\}. \tag{3.23}$$

The integral 3.21 is an important part of the path integral Monte Carlo method, and in chapter 6 we address some aspects of its numerical evaluation. As was the case with the real time kernel, equation 3.21 does not directly hold for actions with the Coulomb potential.

Note that many conventional properties of real-time dynamics do not apply in the imaginary time. For example, $\frac{\mathrm{d}\boldsymbol{r}}{\mathrm{d}\tau}$ is not a velocity, and the center of mass is not conserved.

3.3 Illustration of an imaginary time path

To illustrate what one imaginary time path may look like, an example path of a hydrogen molecule is plotted in figure 3.1, where the path is discretized with a low number of sections $M = 32$. We are interested in the expectation values of equation 3.15, which utilizes the diagonal term of the density matrix $\rho\left(R, R, \beta\right)$, and so, the path starts and ends in the same position. The path of each particle is a loop, and the path of a full system is a set of loops. Note that electrons are more spread out than protons, because lower mass allows higher ”velocities” in the imaginary time.

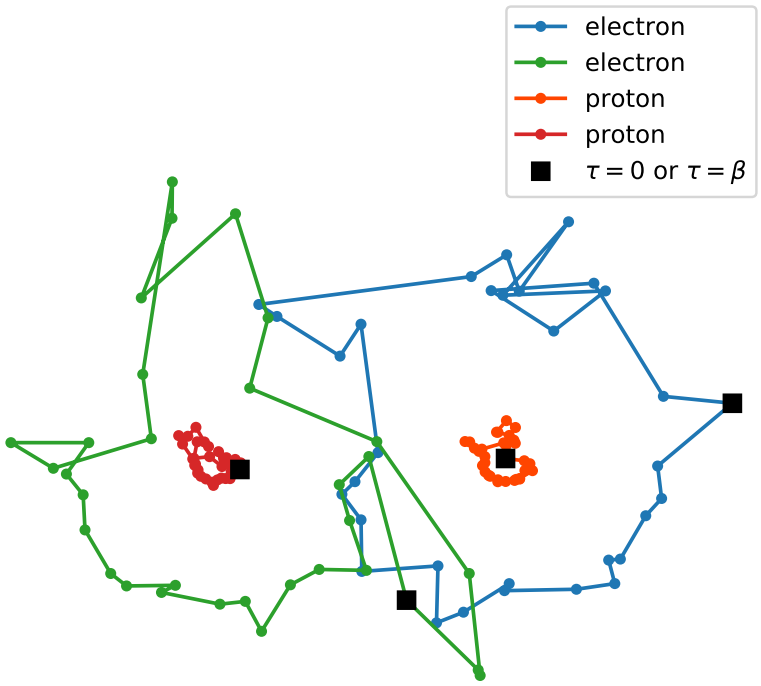

Figure 3.1. *A schematic illustration of imaginary time path for hydrogen molecule* H_2 *near the thermal equilibrium. The path is discretized with a low number of segments. The dots present points, where the particle interactions are evaluated, whereas the solid lines indicate kinetic leaps based on the short time step kernel. The black squares indicate the position* $R_0 = R_M$ *in equation 3.21.*

3.4 Calculation of properties

In this section we derive formulas for the expectation values of observable properties based on the imaginary-time path integrals. The expectation value of equation 3.16 can be discretized similarly to equation 3.21 with

$$\mathrm{Tr}\left[\hat{\rho}_\beta \hat{O}\right] = \int \mathrm{d}R_0 \, \langle R_0 | \hat{\rho}_\beta \hat{O} | R_0 \rangle \tag{3.24}$$

$$= \lim_{M\to\infty} \left(\int \mathrm{d}R_0 \, \langle R_0 | (\hat{\rho}_{\Delta\tau})^M \hat{O} | R_0 \rangle \right) \tag{3.25}$$

$$= \lim_{M\to\infty} \left(\int\int \mathrm{d}R_0 \mathrm{d}R_M \, \langle R_0 | (\hat{\rho}_{\Delta\tau})^M | R_M \rangle \, \langle R_M | \hat{O} | R_0 \rangle \right) \tag{3.26}$$

$$= \lim_{M\to\infty} \left(\int \cdots \int \mathrm{d}R_M \prod_{m=0}^{M-1} \mathrm{d}R_m \, \rho\left(R_m, R_{m+1}, \Delta\tau\right) \, \langle R_M | \hat{O} | R_0 \rangle \right). \tag{3.27}$$

Let us assume that an observable $\hat{O}$ is diagonal in the position basis, which means that it can be evaluated from the sole knowledge of the particle coordinates. For example, potential energy $V(R)$ is a diagonal quantity, but magnetic moment $\boldsymbol{m}(\dot{R}, R) = \sum_i \frac{q_i}{2}(\boldsymbol{r}_i \times \dot{\boldsymbol{r}}_i)$ is not, as it requires knowledge of the velocity. Because $\hat{O}$ is diagonal, the matrix element $\langle R_M | \hat{O} | R_0 \rangle$ can be written with the Dirac's delta function as $O(R_0)\delta\left(R_M, R_0\right)$.

Equation 3.27 becomes

$$\mathrm{Tr}\left[\hat{\rho}_\beta \hat{O}\right] = \lim_{M\to\infty}\left(\int\cdots\int\prod_{m=0}^{M-1}\mathrm{d}R_m\;\rho\left(R_m, R_{m+1}, \Delta\tau\right)O(R_0)\right), \tag{3.28}$$

where $R_M = R_0$.

The observation at a single time slice $O(R_0)$ can be averaged over all the time slices as

$$\mathrm{Tr}\left[\hat{\rho}_\beta \hat{O}\right] = \lim_{M\to\infty}\left(\int\cdots\int\prod_{m=0}^{M-1}\mathrm{d}R_m\;\rho\left(R_m, R_{m+1}, \Delta\tau\right)\frac{1}{M}\sum_{m=0}^{M}O(R_m)\right), \tag{3.29}$$

because the time slices are equivalent in imaginary time [1, p. 335]. This is equivalent to

$$\mathrm{Tr}\left[\hat{\rho}_\beta \hat{O}\right] = \int\mathrm{d}R_0\int_{R'(0)=R_0}^{R'(\beta)=R_0}\mathcal{D}R'(\tau)\;\mathcal{A}e^{-S'[R'(\tau)]}\widetilde{O}\left[R'(\tau)\right], \tag{3.30}$$

where

$$\widetilde{O}\left[R'(\tau)\right] = \frac{1}{\beta}\int_0^\beta \mathrm{d}\tau O\left(R'(\tau)\right) \tag{3.31}$$

is a time-averaged functional corresponding to operator $\hat{O}$. The equation 3.30 appears now in same format as 2.61, so it can be expressed with using the transition element notation

$$\mathrm{Tr}\left[\hat{\rho}_\beta \hat{O}\right] = \int\mathrm{d}R\left\langle R(\beta)\middle|\widetilde{O}\left[R'(\tau)\right]\middle|R(0)\right\rangle. \tag{3.32}$$

Similar to the transition element notation, a new notation is defined for the trace of the transition element, which is

$$\mathrm{Tr}\left[\hat{\rho}_\beta \hat{O}\right] \equiv \mathrm{Tr}_\beta\left[\widetilde{O}\left[R'(\tau)\right]\right]_{S'}. \tag{3.33}$$

Note that Tr_β notation on the right-hand side takes a functional as the input parameter, and it is not a trace operation in a common sense.

To summarize, if an observable depends solely on the positional coordinates, that is $\hat{O}\left|R\right\rangle = O(R)\left|R\right\rangle$, then its thermal expectation value can be calculated with imaginary time path integral

$$\langle O\rangle = \frac{1}{Z}\,\mathrm{Tr}_\beta\left[\widetilde{O}\left[R'(\tau)\right]\right]_{S'}. \tag{3.34}$$

However, this equation is also valid for some observables $O(\dot{R}, R)$ that involve the velocity. In this case, the function $O(\dot{R}, R)$ needs to be derived from the partition function, and it may not be exactly the same as in the classical system. A well-behaved example of a velocity-dependent observable is the magnetic dipole moment, which happens to be a direct imaginary time transformation from the corresponding classical quantity.

The expectation value of the squared magnetic dipole moment is derived in this work. An ill-behaved example of a velocity-dependent observable is the kinetic energy, whose classical correspondent $\frac{1}{2}m\dot{\boldsymbol{r}}^2$ does not apply [1, p. 336], as the square velocity of the path is unbounded in the limit $\Delta\tau \to 0$ [8, p. 177].

4 STATIC SUSCEPTIBILITY

The susceptibility of a system is a measure of how strongly the system responds to an external perturbation, such as an external field. For example, an electric susceptibility measures how much an electric field polarizes the system. Similarly, the magnetic susceptibility describes how much an external magnetic field magnetizes the system.

When discussing the theory of susceptibility, it is common to cover both a static and a dynamic susceptibility, which correspond to time-independent and time-dependent cases, respectively. The main focus of this work is in static susceptibility, but a derivation of dynamic susceptibility is also discussed in appendix A.

Here we derive a general representation of the static susceptibility by utilizing imaginary-time path integrals. In section 4.1 we derive the susceptibility in terms of a partition function Z. In section 4.3 we further derive how these terms can be calculated as functionals of a path integral.

4.1 Classical thermodynamics

Thermodynamical systems at constant temperature and volume minimize a quantity called the Helmholtz free energy. The Helmholtz free energy $\mathcal{F}$ links to the partition function with

$$Z = e^{-\beta \mathcal{F}} \tag{4.1}$$

$$\Leftrightarrow \mathcal{F} = -\frac{1}{\beta} \ln Z. \tag{4.2}$$

Let a quantity Q be coupled to an external field F such that the difference in Helmholtz free energy is [18, p. 60]

$$\Delta \mathcal{F} = - \langle Q \rangle_F F, \tag{4.3}$$

where $\langle \cdot \rangle_F$ denotes thermal expectation value at $F \neq 0$. This work is focused on the case where F corresponds to the magnitude of a magnetic field along some coordinate axis, and Q corresponds to the magnetic dipole moment along that same axis.

The expectation value of Q can be evaluated with [18, p. 60]

$$\langle Q \rangle_F = - \left(\frac{\partial \mathcal{F}}{\partial F} \right). \tag{4.4}$$

Static susceptibility χ determines linear coupling between $\langle Q \rangle_F$ and F with

$$\langle Q \rangle_F = \chi F. \tag{4.5}$$

The susceptibility is a function of F, but usually only the limit $F \to 0$ is considered. The zero-field susceptibility is [3, p. 41][18, p. 66]

$$\chi = \lim_{F \to 0} \left(\frac{\partial \langle Q \rangle_F}{\partial F} \right). \tag{4.6}$$

This can be written with equations 4.4 and 4.2 as

$$\langle Q \rangle_F = -\frac{\partial}{\partial F} \left(-\frac{1}{\beta} \ln Z \right) \tag{4.7}$$

$$= \frac{1}{\beta Z} \frac{\partial Z}{\partial F}. \tag{4.8}$$

Plugging 4.8 to 4.6 gives the susceptibility in terms of the partition function

$$\chi = \frac{1}{\beta} \lim_{F \to 0} \left(\frac{\partial}{\partial F} \left(\frac{1}{Z} \frac{\partial Z}{\partial F} \right) \right) \tag{4.9}$$

$$= \frac{1}{\beta} \lim_{F \to 0} \left(\frac{-1}{Z^2} \frac{\partial Z}{\partial F} \frac{\partial Z}{\partial F} + \frac{1}{Z} \frac{\partial^2 Z}{\partial F^2} \right) \tag{4.10}$$

$$= \frac{1}{\beta} \left(\frac{-1}{Z^2} \lim_{F \to 0} \left(\frac{\partial Z}{\partial F} \right)^2 + \frac{1}{Z} \lim_{F \to 0} \left(\frac{\partial^2 Z}{\partial F^2} \right) \right). \tag{4.11}$$

Now that the susceptibility is expressed with partial derivatives of the partition function, the next step is to find these derivatives.

4.2 Action

The system described earlier has the classical Lagrangian

$$L\left(\dot{R}, R\right) = L_0\left(\dot{R}, R\right) + Q\left(\dot{R}, R\right) F, \tag{4.12}$$

where L_0 is the Lagrangian at $F = 0$. The imaginary-time action from equation 3.19 is

$$S'[R'(\tau)] = -\int_0^\beta \mathrm{d}\tau \, L\left(\frac{1}{-\mathrm{i}\hbar} \frac{\mathrm{d}R'(\tau)}{\mathrm{d}\tau}, R'(\tau) \right)$$

$$= S'_0 - \beta \frac{1}{\beta} \int_0^\beta \mathrm{d}\tau \, Q\left(\frac{1}{-\mathrm{i}\hbar} \frac{\mathrm{d}R'(\tau)}{\mathrm{d}\tau}, R'(\tau) \right) F \tag{4.13}$$

$$= S'_0 - \beta \widetilde{Q}[R'(\tau)] F \tag{4.14}$$

$$= S'_0 + S'_F \tag{4.15}$$

where S'_0 is the action of the system in the absence of the field, S'_F is a perturbed part of the action, and $\widetilde{Q}$ is a time-averaged functional.

4.3 Susceptibility estimator

Partial derivatives in equation 4.11 can now be evaluated. Partition function 3.14 can be written in terms of equation 3.33 as

$$Z = \mathrm{Tr}_\beta \left[1\right]_{S'} \tag{4.16}$$

$$= \int \mathrm{d}R_0 \int_{R'(0)=R_0}^{R'(\beta)=R_0} \mathcal{D}R'(\tau)\ \mathcal{A} e^{-S'[R'(\tau)]} \tag{4.17}$$

$$= \mathrm{Tr}_\beta \left[e^{-S'_F}\right]_{S'_0}, \tag{4.18}$$

where the amplitude has been split into two parts $e^{-S'} = e^{-S'_0} e^{-S'_F}$. The equation 4.18 tells that the partition function of perturbed system can be evaluated with the functional $e^{-S'_F}$ in the unperturbed system [8, p. 166]. This is possible, because the normalization constant $\mathcal{A}$ is the same on both the unperturbed and the perturbed system. The amplitude can be expanded in the exponential series

$$e^{-S'_F} = 1 \ + \ \left(-S'_F\right) \ + \ \frac{1}{2}\left(-S'_F\right)^2 \ + \ \cdots \tag{4.19}$$

$$= 1 \ + \ \beta \widetilde{Q}\left[R'(\tau)\right] F \ + \ \frac{1}{2}\left(\beta \widetilde{Q}\left[R'(\tau)\right] F\right)^2 \ + \ \cdots, \tag{4.20}$$

which can be plugged into equation 4.18, giving

$$Z = \mathrm{Tr}_\beta \left[1\right]_{S'_0} \ + \ \beta\, \mathrm{Tr}_\beta \left[\widetilde{Q}\right]_{S'_0} F \ + \ \frac{1}{2}\left(\beta^2\, \mathrm{Tr}_\beta \left[\widetilde{Q}^2\right]_{S'_0}\right) F^2 \ - \ \cdots. \tag{4.21}$$

This expression is the Taylor expansion of $Z(F)$ around $F = 0$, and so the second and the third term gives the partial derivatives required by equation 4.11

$$\lim_{F\to 0}\left(\frac{\partial Z}{\partial F}\right) = \beta\, \mathrm{Tr}_\beta \left[\widetilde{Q}\right]_{S'_0} \tag{4.22}$$

$$\lim_{F\to 0}\left(\frac{\partial^2 Z}{\partial F^2}\right) = \beta^2\, \mathrm{Tr}_\beta \left[\widetilde{Q}^2\right]_{S'_0}. \tag{4.23}$$

The susceptibility 4.11 becomes

$$\chi = \frac{1}{\beta}\left(\frac{-1}{Z^2}\left(\beta\, \mathrm{Tr}_\beta \left[\widetilde{Q}\right]_{S'_0}\right)^2 + \frac{1}{Z}\beta^2\, \mathrm{Tr}_\beta \left[\widetilde{Q}^2\right]_{S'_0}\right) \tag{4.24}$$

$$= \beta\left(\left\langle \widetilde{Q}^2 \right\rangle - \left\langle \widetilde{Q} \right\rangle^2\right), \tag{4.25}$$

where equation 3.34 is applied on the last line. This can be also written as

$$\chi = \beta\left\langle \left(\widetilde{Q}^2 - \left\langle \widetilde{Q} \right\rangle\right)^2 \right\rangle, \tag{4.26}$$

which states that susceptibility against F depends on the fluctuation of $\widetilde{Q}$ in the equilibrium. Therefore, the response to external field can be calculated without direct simula-

tions of that field. The equation 4.25 is related to the well-known *fluctuation–dissipation theorem* [19, p. 23].

5 MAGNETIC SUSCEPTIBILITY

There are many forms of magnetism. When an external magnetic field is applied to a material, it induces magnetic dipole moments opposing the field, which is the source of the diamagnetism. On the other hand, the imposed field also aligns permanent dipole moments parallel to the field, which is the source of the paramagnetism. The largest contribution of the paramagnetism originates from the magnetic dipole moment of the electron spins. Some materials are capable of pertaining the magnetization even without the presence of external field, which is known as *ferromagnetism*. With ferromagnetism, the permanent dipole moments are collectively aligned by exchange interactions between the dipoles. [19]

Noble gases are the only substances that have fully diamagnetic electronic structures. That is, no paramagnetism is present in the noble gases. There are many other substances that are mainly diamagnetic. One such example is the hydrogen molecule, for which the opposing electron spins cancel each other out, leaving the paramagnetic contribution to be about 2% [6]. By assuming that the paramagnetic contribution is negligible, the total magnetic susceptibility can be estimated by using only the diamagnetic contribution.

In this chapter we express the diamagnetic susceptibility with imaginary-time path integrals. Section 5.1 presents magnetic susceptibility in terms of a general susceptibility, which was derived in the previous chapter. Section 5.2 presents magnetic dipole moment as a functional, which is used to derive the final equation for the magnetic susceptibility. The derived equation corresponds to the one obtained from references [1, 20].

An alternative representation of the susceptibility is presented in appendix B, where operator formalism is used to derive the exact diamagnetic susceptibility for the hydrogen atom with a fixed nucleus.

5.1 Representation with general susceptibility

In this section, we write magnetic susceptibility in terms of the general susceptibility. Let $\boldsymbol{m}$ be the magnetic moment of a system, and let the system be affected by an external magnetic field, which has magnetic flux density $\boldsymbol{B}$. Quantities Q and F now correspond to m_i and B_i respectively, where $i \in \{x, y, z\}$ denote the coordinate components of a

vector quantity. The difference in Helmholtz free energy is given by equation 4.3 as

$$\Delta\mathcal{F} = -\left\langle \boldsymbol{m} \right\rangle_{\boldsymbol{B}} \cdot \boldsymbol{B}. \tag{5.1}$$

If the magnetization $\boldsymbol{M} = \frac{\langle \boldsymbol{m} \rangle}{V}$ is small, then

$$\boldsymbol{B} = \mu_0 \left(\boldsymbol{H} + \boldsymbol{M} \right) \approx \mu_0 \boldsymbol{H}, \tag{5.2}$$

where μ_0 is the magnetic permeability of the vacuum. The magnetic moment is given directly by equation 4.4, and it is [19, p. 21]

$$\left\langle m_i \right\rangle_{B_i} = -\frac{\partial \mathcal{F}}{\partial B_i}. \tag{5.3}$$

The general susceptibility is given by equation 4.6, but it differs from the common definition of the magnetic susceptibility, which is [19, p. 23]

$$\chi_i^{\mathrm{mag}} = \lim_{H_i \to 0} \left(\frac{\partial \left\langle m_i \right\rangle_{H_i}}{\partial H_i} \right). \tag{5.4}$$

Where the general susceptibility χ_i is defined as a derivative of B_i, the magnetic susceptibility χ^{mag} is defined as a derivative of H_i instead. This slight difference brings an extra term μ_0 to the magnetic susceptibility as

$$\chi_i^{\mathrm{mag}} = \mu_0 \chi_i. \tag{5.5}$$

5.2 Susceptibility estimator

This section shows how the magnetic susceptibility is calculated by using the general susceptibility equation 4.25. Magnetic moment may seem problematic, as it depends on particle velocities, which is not directly supported by equation 3.34. However, the problem is avoided, because the magnetic moment functional can be expressed without instantaneous particle velocities or time-dependence.

The Lagrangian of system is given by equation 2.39 as

$$L\left(\dot{R}, R\right) = L_0\left(\dot{R}, R\right) + \boldsymbol{m}\left(\dot{R}, R\right) \cdot \boldsymbol{B},$$

which gives imaginary-time action 4.14 as

$$S'[R'(\tau)] = S'_0 - \beta \widetilde{\boldsymbol{m}}[R'(\tau)] \boldsymbol{B}, \tag{5.6}$$

where

$$\widetilde{\boldsymbol{m}}\left[R(t)\right] = \frac{1}{\beta} \int_0^\beta \mathrm{d}\tau \sum_n^N \frac{q_n}{2} \left(\boldsymbol{r}_n \times \left(\frac{1}{-\mathrm{i}\hbar} \frac{\mathrm{d}\boldsymbol{r}_n}{\mathrm{d}\tau} \right) \right) \tag{5.7}$$

is the time-averaged magnetic moment of the trajectory. Using a change of integration variable $\mathrm{d}\tau \frac{\mathrm{d}\boldsymbol{r}_n}{\mathrm{d}\tau} = \mathrm{d}\boldsymbol{r}_n$, the functional becomes

$$\widetilde{\boldsymbol{m}}\left[R'(\tau)\right] = \frac{\mathrm{i}}{\hbar\beta} \sum_n^N \frac{q_n}{2} \oint_{\partial\mathcal{S}_n} \boldsymbol{r}_n \times \mathrm{d}\boldsymbol{r}_n, \tag{5.8}$$

where $\partial\mathcal{S}_n$ is a closed imaginary-time trajectory of particle n. Let $\mathcal{S}_n$ be some filling surface of the trajectory. Applying the Stokes' theorem yields

$$\widetilde{\boldsymbol{m}}\left[R'(\tau)\right] = \frac{\mathrm{i}}{\hbar\beta} \sum_n^N q_n \boldsymbol{\mathcal{A}}_n, \tag{5.9}$$

where $\boldsymbol{\mathcal{A}}_n$ is a "vector area" of the surface $\mathcal{S}_n$. A component $\mathcal{A}_{n,i}$ is formed by projecting the surface $\mathcal{S}_n$ along a coordinate axis i. Area $\mathcal{A}_{n,i}$ can be negative depending on the choice of handedness. Note that unlike the instantaneous magnetic moment, this functional does not depend on particle velocities.

If a practical computation of vector area is considered, it is evaluated most efficiently by discretizing the closed integral 5.8 with

$$\boldsymbol{\mathcal{A}}_n = \frac{1}{2} \sum_{m=1}^M \boldsymbol{r}_{n,m} \times (\boldsymbol{r}_{n,m} - \boldsymbol{r}_{n,m-1}) \tag{5.10}$$

where index m corresponds to a time slice of the path, and $\boldsymbol{r}_{n,0} = \boldsymbol{r}_{n,M}$.

The magnetic susceptibility is given by equations 4.25 and 5.5 as

$$\chi_i^{\mathrm{mag}} = \mu_0\beta \left(\left\langle \widetilde{m}_i^2 \right\rangle - \left\langle \widetilde{m}_i \right\rangle^2 \right). \tag{5.11}$$

Rotationally invariant systems have $\left\langle \widetilde{m}_i \right\rangle = 0$. Plugging in functional 5.9 gives the final expression for the susceptibility [1, 20]

$$\chi_i^{\mathrm{mag}} = -\frac{\mu_0}{\hbar^2\beta} \left\langle \left(\sum_n^N q_n \mathcal{A}_{n,i} \right)^2 \right\rangle. \tag{5.12}$$

This gives only the diamagnetic contribution, because the magnetic moment functional 5.7 takes only into account the dynamics of charged particles and not the spin.

6 PATH INTEGRAL MONTE CARLO METHOD

In this section we show how imaginary-time path integrals are evaluated in practice with the Path integral Monte Carlo method (PIMC). In principle, the integrals comprise an infinite number of paths to evaluate. Fortunately, a finite number of random samples can be used to estimate the integrals at a decent and controllable accuracy. A path can be approximated with discrete line segments, and sum over all possible paths can be estimated with a finite number of Monte Carlo path samples [3, p. 55]. Also, random sampling can be made more efficient by importance sampling, which increases the significance of the samples by drawing them from the vicinity of the classical path.

6.1 Monte Carlo method

The path integral is essentially a high-dimensional integral. Common grid integration methods are insufficient for the task, and so, the integral is evaluated with Monte Carlo importance sampling. Let us write an integrand $g(\boldsymbol{x})$ with a chosen probability distribution $P(\boldsymbol{x})$ as

$$\int g(\boldsymbol{x})\mathrm{d}\boldsymbol{x} = \int P(\boldsymbol{x})\frac{g(\boldsymbol{x})}{P(\boldsymbol{x})}\mathrm{d}\boldsymbol{x}. \tag{6.1}$$

This integral is then interpreted as the expectation value [21, p. 92][22]

$$\int g(\boldsymbol{x})\mathrm{d}\boldsymbol{x} = \left\langle \frac{g(\boldsymbol{x})}{P(\boldsymbol{x})} \right\rangle_P \tag{6.2}$$

$$\approx \frac{1}{N}\sum_{i=1}^{N}\frac{g(\boldsymbol{x}_i)}{P(\boldsymbol{x}_i)}, \tag{6.3}$$

where $\langle\cdot\rangle_P$ denotes that a variable $\boldsymbol{x}$ is distributed by P, and where samples $\boldsymbol{x}_i$ are also distributed by the P. The probability distribution P must be such a function that can generate samples $\boldsymbol{x}_i$ efficiently. The closer the fraction $\frac{g}{P}$ is to a constant, the more accurate the discrete sum is. Therefore, a good choice of P is essential for sampling efficiency.

6.2 Markov chain Monte Carlo

In essence, PIMC evaluates the high-dimensional integrals given in equation 3.29. One sample of Monte Carlo is a trajectory of all particles [3, p. 62]. However, there is a slight challenge in calculation of expectation value 3.16, because it depends on partition the function Z, which by itself is a laborious path integral. This is where the *Markov chain Monte Carlo* [21, pp. 268–271] is useful, as it brings relatively efficient sampling in high dimensions, while it also does not require normalization of the partition function.

The markov chain Monte Carlo draws random samples $\boldsymbol{x}_{i+1}$ by using information from the previously drawn sample $\boldsymbol{x}_i$, which forms a random walker. Consecutive steps are highly correlated, and so samples can be separated with multiple steps. The sampling is made efficient by favouring those steps that increase the probability of walker $P(\boldsymbol{x}_i)$. The walker should be given enough time to converge to the equilibrium of the probability distribution, and the non-converged samples should be discarded. If equilibrium convergence is not established, initial walker position may form a bias in sample mean.

Even though PIMC is an exact method in theory, the insufficient number of walker steps may render a bias in practice. Given simulation time should be always long enough for random walker to find the equilibrium. If the applied simulation time is short, the true equilibrium may be hard to tell apart from a local minimum. This is larger concern with complex systems, because they require high number of samples, which is heavy on computational resources. Generally speaking, the relative computational cost of a PIMC simulation increases by the following factors:

- particle count,
- low temperature,
- short time step $\Delta\tau$,
- heavy nucleus, and
- indistinguishability of electrons.

The last factor, indistinguishability of electrons, is not a concern in this work.

6.3 Estimation of statistical error

Integrated quantities are associated with a statistical uncertainty due to the finite number of random samples. The margin of error is usually presented with the *standard error of the mean* (SEM), which for uncorrelated samples is

$$\mathrm{SEM} = \frac{\sigma}{\sqrt{N}}, \tag{6.4}$$

where σ is the standard deviation of the samples. However, if the subsequent samples are correlated, this underestimates the error. The SEM can be adjusted to take sample

correlation into account with

$$\mathrm{SEM} = \frac{\sigma}{\sqrt{N_{\mathrm{eff}}}}, \tag{6.5}$$

where N_{eff} is the effective sample size. It can be estimated with [21, p.500]

$$N_{\mathrm{eff}} = N \left(1 + 2 \sum_{n=1}^{N} C_n \right)^{-1} \tag{6.6}$$

where C_n is the autocorrelation of the subsequent samples. The autocorrelation is [2]

$$C_n = \frac{1}{(N-n)\,\sigma^2} \sum_{i=1}^{N-n} \Big(\big(f_i - \langle f \rangle \big) \big(f_{i+n} - \langle f \rangle \big) \Big), \tag{6.7}$$

where $f_i = \frac{g(\boldsymbol{x}_i)}{P(\boldsymbol{x}_i)}$ are the samples. All margins of error in this work correspond to 2 SEM confidence.

6.4 Metropolis–Hastings algorithm

The Markov chain Monte Carlo is most commonly utilized with some variation of a *Metropolis–Hastings algorithm*. The Metropolis–Hastings algorithm implements a walker that samples the equilibrium by fulfilling the conditions of *detailed balance*. In detailed balance, transitions rates between states are equal to both directions, and so the population of states does not change. That is, [3]

$$P(\boldsymbol{x}_i) P(\boldsymbol{x}_i \to \boldsymbol{x}_{i+1}) = P(\boldsymbol{x}_{i+1}) \Pr(\boldsymbol{x}_{i+1} \to \boldsymbol{x}_i), \tag{6.8}$$

where $P(\boldsymbol{x}_i)$ is the probability of state $\boldsymbol{x}_i$, and $P(\boldsymbol{x}_i \to \boldsymbol{x}_{i+1})$ is the probability of transition $\boldsymbol{x}_i \to \boldsymbol{x}_{i+1}$. The detailed balance is maintained by splitting the step generation into two parts. First, a move candidate $\boldsymbol{x}_{i+1}$ is generated, and then it is accepted with a certain probability. If the move is accepted, then $\boldsymbol{x}_{i+1}$ becomes the value of the next step. If it is not accepted, then the old state is chosen as the value of the next step, meaning $\boldsymbol{x}_{i+1} = \boldsymbol{x}_i$. The transition probability can be written

$$P(\boldsymbol{x}_i \to \boldsymbol{x}_{i+1}) = T(\boldsymbol{x}_i \to \boldsymbol{x}_{i+1}) A(\boldsymbol{x}_i \to \boldsymbol{x}_{i+1}) \tag{6.9}$$

where $T(\boldsymbol{x}_i \to \boldsymbol{x}_{i+1})$ is the probability of the proposal and $A(\boldsymbol{x}_i \to \boldsymbol{x}_{i+1})$ is the probability of acceptance. Plugging 6.9 to 6.8, one can find that

$$A(\boldsymbol{x}_i \to \boldsymbol{x}_{i+1}) = \min\left(1,\ q(\boldsymbol{x}_i \to \boldsymbol{x}_{i+1})\right) \tag{6.10}$$

is a valid acceptance probability, where unconstrained acceptance probability is

$$q(\boldsymbol{x}_i \to \boldsymbol{x}_{i+1}) = \frac{T(\boldsymbol{x}_{i+1} \to \boldsymbol{x}_i) P(\boldsymbol{x}_{i+1})}{T(\boldsymbol{x}_i \to \boldsymbol{x}_{i+1}) P(\boldsymbol{x}_i)}. \tag{6.11}$$

So, in essence, the Metropolis–Hastings algorithm generates samples from the equilibrium by accepting new steps with the probability 6.10. If $q \leq 1$, the move is always accepted, which favours states of high probability. Note that the probability distribution $P(\boldsymbol{x}_i)$ needs not be normalized to evaluate the fraction in q.

6.5 Path sampling

In PIMC calculations, the state $\boldsymbol{x}_i$ corresponds to an imaginary-time trajectory $R'(\tau) \approx [R_1, \dots R_M]$. The probability of state $P(\boldsymbol{x}_i)$ is obtained by interpreting the probability amplitude $e^{-S'[R'(\tau)]}$ as a Boltzmann's coefficient $e^{-\beta E^{\text{eff}}[R'(\tau)]}$, where E^{eff} is an effective potential energy of the trajectory [17]. By favouring steps that decrease the action $S'[R'(\tau)]$, the walker is brought to the vicinity of the classical path.

The probability amplitude from equation 3.18 can be written

$$\mathcal{A}e^{-S'[R'(\tau)]} = \lim_{M\to\infty} \prod_{m=0}^{M-1} A e^{-S'(R_m, R_{m+1}, \Delta\tau)}. \tag{6.12}$$

The term $S'(R_m, R_{m+1}, \Delta\tau)$ can be expressed similarly as in equation 3.23

$$\begin{aligned} S'(R_m, R_{m+1}, \Delta\tau) &= -\Delta\tau\, L\left(\frac{R_{m+1} - R_m}{-\mathrm{i}\hbar\Delta\tau}, R_m\right) && (6.13)\\ &= \Delta\tau \left(\sum_n^N \frac{m_n}{2\hbar^2} \frac{\left(\boldsymbol{r}_{n,m+1} - \boldsymbol{r}_{n,m}\right)^2}{\Delta\tau^2} + \sum_{n'>n}^N V\left(\boldsymbol{r}_{n,m}, \boldsymbol{r}_{n',m}\right)\right) && (6.14)\\ &= \Delta\tau \left(\sum_n^N \mathcal{K}_{n,m} + \sum_{n'>n}^N V_{n,n',m}.\right) && (6.15)\\ &= \Delta\tau E_m^{\text{eff}}, && (6.16) \end{aligned}$$

where terms $\mathcal{K}$ and E^{eff} can be interpreted as the kinetic energy and an effective energy of the time step. The probability amplitude 6.12 becomes

$$\begin{aligned} \mathcal{A}e^{-S'[R'(\tau)]} &= \lim_{M\to\infty} \prod_{m=0}^{M-1} A e^{-\Delta\tau E_m^{\text{eff}}} && (6.17)\\ &= \mathcal{A}e^{-\beta E^{\text{eff}}[R'(\tau)]} && (6.18)\\ &\propto P(\boldsymbol{x}_i), \end{aligned}$$

The term $E^{\text{eff}}[R'(\tau)]$ is real-valued, and it can be thought of as an effective energy of whole "path polymer". Because the amplitude $e^{-\beta E^{\text{eff}}}$ is non-negative, it can be interpreted as the Boltzmann coefficient. [17]

Consider a transition of path that affects only one particle n at time slice m. In the product 6.17, most of the terms remain constant, as only the terms E_{m-1}^{eff} and E_m^{eff} depend on R_m. If 6.17 is substituted to acceptance probability 6.11, the constant terms cancel,

giving

$$q(\boldsymbol{x}_i \to \boldsymbol{x}_{i+1}) = \frac{T(\boldsymbol{x}_{i+1} \to \boldsymbol{x}_i) e^{-\Delta\tau\left(E'^{\text{eff}}_{m-1} + E'^{\text{eff}}_{m}\right)}}{T(\boldsymbol{x}_i \to \boldsymbol{x}_{i+1}) e^{-\Delta\tau\left(E^{\text{eff}}_{m-1} + E^{\text{eff}}_{m}\right)}},$$

where E'^{eff} and E^{eff} notate energy in proposed position $\boldsymbol{x}_{i+1}$ and current position $\boldsymbol{x}_i$ respectively. Similarly, equation 6.15 shows that the terms that do not contain n, remain constant in the transition, and so the acceptance probability 6.11 becomes

$$\begin{aligned} q(\boldsymbol{x}_i \to \boldsymbol{x}_{i+1}) &= \frac{T(\boldsymbol{x}_{i+1} \to \boldsymbol{x}_i) e^{-\Delta\tau\left(\mathcal{K}'_{n,m-1} + \mathcal{K}'_{n,m} + \sum_{n'} V'_{n,n',m}\right)}}{T(\boldsymbol{x}_i \to \boldsymbol{x}_{i+1}) e^{-\Delta\tau\left(\mathcal{K}_{n,m-1} + \mathcal{K}_{n,m} + \sum_{n'} V_{n,n',m}\right)}} \\ &= \frac{T(\boldsymbol{x}_{i+1} \to \boldsymbol{x}_i)}{T(\boldsymbol{x}_i \to \boldsymbol{x}_{i+1})} e^{-\Delta\tau(\Delta\mathcal{K} + \Delta V)}. \end{aligned}$$

This means that a full trajectory does not need to be evaluated for the calculation of q, but only the changed interactions need to be re-evaluated.

The computation time of q can be reduced even further by cleverly choosing the transition function. Note that a free particle kernel 2.29 is a Gaussian function in imaginary time. If T is chosen as the 3-dimensional Gaussian distribution with variance $\frac{\hbar^2}{2m_n}\Delta\tau$, then [2]

$$\frac{T(\boldsymbol{x}_{i+1} \to \boldsymbol{x}_i)}{T(\boldsymbol{x}_i \to \boldsymbol{x}_{i+1})} e^{-\Delta\tau\Delta\mathcal{K}} = 1, \tag{6.19}$$

which leads to the transition probability

$$q(\boldsymbol{x}_i \to \boldsymbol{x}_{i+1}) = e^{-\Delta\tau\Delta V}. \tag{6.20}$$

This means that the kinetic energy does not need to be sampled at all, and it is known as *bisection method*.

6.6 Symmetry considerations

Indistinguishable particles pose some challenges in the sampling process. The density matrix of indistinguishable fermions and bosons is [17]

$$\rho_{F/B}(R_a, R_b, \beta) = \frac{1}{N!} \sum_{\mathcal{P}} (\mp 1)^{\mathcal{P}} \int_{R'(0)=R_a}^{R'(\beta)=\mathcal{P}R_b} \mathcal{D}R'(\tau)\, \mathcal{A} e^{-S'[R'(\tau)]}. \tag{6.21}$$

where $\mathcal{P}$ denotes a permutation of indistinguishable particle labels, and signs $-$ and $+$ correspond to fermions and bosons respectively. Effectively, the summation of permutations connects trajectories of different particles forming longer shared trajectories. The sum over permutations can be sampled with Monte Carlo along with the sampling of paths.

In case of fermions, the minus sign in equation 6.21 poses a problem in sampling. The

probability amplitude of combined path may be negative, which can not be directly interpret as a probability. There are methods to circumvent this [2, 17], but they are computationally complex to calculate. The problem is known as the *fermion sign problem*, which is proven to be NP-hard [3, p. 72], meaning that there does not exist a computationally efficient method for it.

The symmetry of fermions and bosons is not considered in this work, as all of the inspected systems contain only distinguishable particles. For example, the particles forming the hydrogen molecule are distinguishable when both two protons and two electrons are assumed to have opposing spins. If the overlap of the identical particles is negligible, the indistinguishability need not be considered.

6.7 PIMC path sample

Even though illustrative example of PIMC path was given in figure 3.1, it does not reflect common simulations in practice, as the number of time slices is usually much higher. Figure 6.1 plots two actual samples from a hydrogen molecule simulation. The number of time slices is 21052 and 2105 for temperatures $300\,\mathrm{K}$ and $3000\,\mathrm{K}$ respectively. At lower temperature, the path of particle is longer, because higher inverse temperature β corresponds to longer imaginary time. A thermal wave length of nucleus is clearly visible, and it increases at lower temperatures.

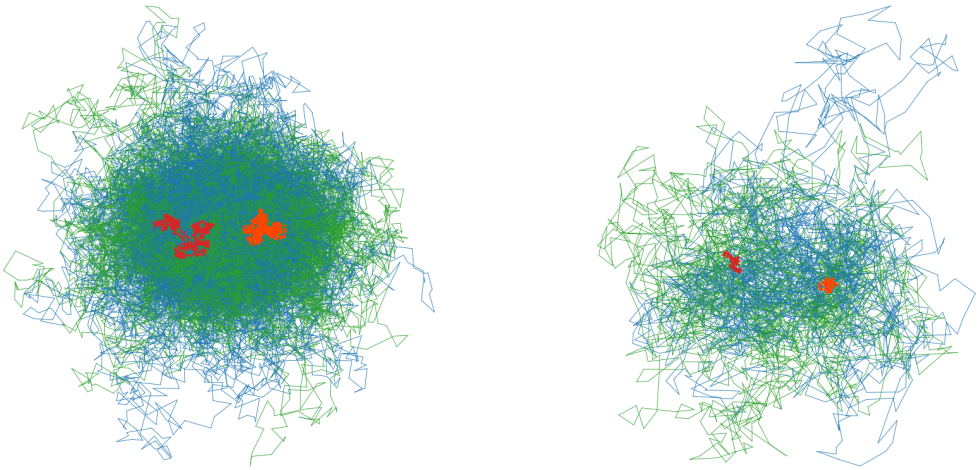

(a) $T = 300\,\mathrm{K}$ ***(b)*** $T = 3000\,\mathrm{K}$

Figure 6.1. *Random path samples of the hydrogen molecule* H_2 *from an actual simulation. Green and blue lines correspond to electrons, and red and orange lines correspond to nuclei.*

7 DIAMAGNETIC SUSCEPTIBILITIES OF LIGHT ATOMS AND MOLECULES

Diamagnetic susceptibilities are studied with PIMC simulations, which are carried out on systems listed in table 7.1. These systems contain light nuclei, which undergo significant nonadiabatic effects. Diatomic molecules, such as H_2, have rotational and vibrational states that are activated by the finite temperature. The isotope effects of the diatomic molecules are inspected by replacing the protons (m_p) by variable nuclear masses including positrons (m_e), deuterons $(2m_\mathrm{p})$, and artificially weighted nuclei ($m_\mathrm{e} - 8m_\mathrm{p}$). The positronic systems represent special interest, because they show the extreme limit of the nonadiabatic effects, which is usually challenging to simulate. The positronic systems are unstable, but they are still relevant in some spectroscopic arrangements.

The inspected systems have no more than two particles of the same kind, so by assuming opposite spins for the identical particles, the indistinguishability does not pose a problem. Fortunately, the ground state of two electron system does have opposite spins. Also, the paramagnetic contribution is cancelled out if the two spins are opposite, and the total magnetic susceptibility is given by the diamagnetic susceptibility. All inspected systems are diamagnetic, except for H and H_2^+.

Energies are measured with the virial energy estimator [2, p. 23], and diamagnetic susceptibilities are measured with the estimator given in equation 5.12. First, the energies

Table 7.1. *List of simulated systems. A positronium is an exotic one-electron system that has a positron in place of its nucleus.*

Symbol	Nucleus	Name	Table E	Table χ	Figure χ
H	AQ/BO	hydrogen atom	7.2	7.3	7.1, 7.2a
$^4\mathrm{He}$	AQ/BO	helium atom	7.2	7.3	7.2b
H_2	AQ/BO	hydrogen molecule	7.2	7.4	7.3a, 7.4
HD	AQ	hydrogen deuteride	7.2	7.5	
D_2	AQ	deuterium molecule	7.2	7.4	7.4
H_2^+	AQ	hydrogen molecule ion	7.2	7.5	
Ps	AQ	positronium atom	7.2	7.5	
Ps_2	AQ	positronium molecule	7.2	7.4	7.4
h_2	AQ	artificial homonuclear diatomic molecules			7.4

are compared to reference values, which shows that simulations are fairly accurate. Then, the susceptibilities are presented. Nonadiabatic *All Quantum* (AQ) nuclei are compared to fixed *Born–Oppenheimer* (BO) nuclei.

Appendix C links additional information of the applied simulations. It includes, *e.g.*, used simulation parameters and more results from other observables. The simulations were carried out using a software developed in our research group [2, 3].

7.1 Unit conversions of the susceptibility

It should be emphasized that this work utilizes the SI convention of magnetism instead of the widely utilized Gaussian convention. The magnetic susceptibility in SI convention is 4π times larger than in Gaussian convention. Also, it should be noted that where previous sections considered susceptibility system-wise, this section presents susceptibilities per mole of gas. SI molar susceptibility has unit $[\frac{\mathrm{m}^3}{\mathrm{mol}}]$, and it can be converted from Gaussian cgs unit $[\frac{\mathrm{cm}^3}{\mathrm{mol}}]$ with

$$\chi_{\mathrm{mol}}^{\mathrm{SI}} = 4\pi \cdot 10^{-6}\ \chi_{\mathrm{mol}}^{\text{cgs (Gaussian)}} \tag{7.1}$$

$$\approx 1.256\,64 \cdot 10^{-5}\ \chi_{\mathrm{mol}}^{\text{cgs (Gaussian)}}. \tag{7.2}$$

Similarly, the conversion factors for the atomic units $[a_0^3]$ are

$$\chi_{\mathrm{mol}}^{\mathrm{SI}} \approx 8.923\,89 \cdot 10^{-8}\ \chi^{\text{a.u. (SI)}} \tag{7.3}$$

$$\approx 1.121\,41 \cdot 10^{-6}\ \chi^{\text{a.u. (Gaussian)}}. \tag{7.4}$$

In this section the susceptibility $\chi_{\mathrm{mol}}^{\mathrm{SI}}$ is denoted with χ.

7.2 Time step length extrapolation

The accuracy of PIMC simulations depends on the time step length parameter $\Delta\tau$. The shorter values of $\Delta\tau$ pose smaller discretization error, while they make calculations computationally heavier. Extrapolation to $\Delta\tau \to 0$ may be required to obtain non-biased estimates. All results presented in this work reflect the limit $\Delta\tau = 0$ estimate.

The time step length is extrapolated at $\Delta\tau = 0$ with a linear fit, which is based on calculations using $\Delta\tau \in \{0.01,\, 0.03,\, 0.05\}$, where the unit of $\Delta\tau$ is an inverse of Hartree energy ${E_\mathrm{h}}^{-1}$. Systems Ps and Ps_2 are exceptions, which are calculated with $\Delta\tau \in \{0.1,\, 0.3,\, 0.5\}$. The longer time steps can be used for Ps and Ps_2, because light nuclei have smaller errors due to the finite time step, which allows the use of the longer time step for increased statistical accuracy.

The susceptibility estimator 5.12 has a strong linear discretization error, which is demonstrated in figure 7.1. The figure also shows linear extrapolation, which is applied for all susceptibility and energy values. In most cases, the energy values are so accurate that

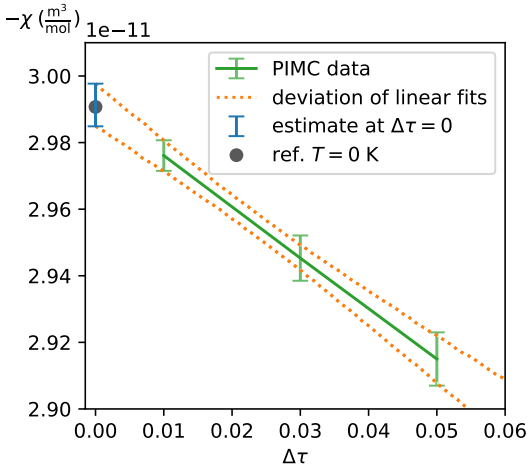

Figure 7.1. *Demonstration of the linear extrapolation, which is used to estimate the observable and the error bar in the limit of $\Delta\tau = 0$. The observable in this case is the susceptibility, which has a virtually linear error with $\Delta\tau$. The system is H (AQ) and the temperature is $T = 3000\,\mathrm{K}$. The extrapolation to $\Delta\tau = 0$ matches the reference value, which is given in table 7.3.*

they are not significantly affected by the extrapolation. The energy of Ps_2 shows nonlinearity within utilized time step values, and as an exception, it is presented with $\Delta\tau = 0.1$ calculation instead of extrapolation.

The statistical uncertainty at $\Delta\tau = 0$ is estimated by resampling the linear extrapolation based on the uncertainties of the data at each time step. First, the margins of error with a finite $\Delta\tau$ calculations are used to generate random samples. A linear regression is applied to each sample individually, and the limit $\Delta\tau = 0$ is extrapolated. A deviation of extrapolations is used to set margins of error for the $\Delta\tau = 0$ estimate. All margins of error are expressed with 2 SEM, which corresponds to 95% confidence.

7.3 Total energy

Total energies of all systems are presented in table 7.2. The energy is a common benchmark quantity, and there is accurate reference data available that can be compared with the PIMC results. Finite temperature PIMC energies can be extrapolated to zero kelvin, where they can be compared to zero kelvin reference values [24–31] from other high-accuracy methods. The PIMC results fit accurately to the reference values, which gives an affirmation to accuracy of the simulations.

Systems H, He and H_2 (BO) show no temperature dependence, as these systems have no nucleus–nucleus interaction. Low temperatures mostly affects nuclear bonds but not the electronic structure. The energies of the diatomic AQ systems H_2, HD, D_2 and H_2^+ increase with the temperature, because rotational and vibrational states of the nuclei are activated.

The dipositronium cannot be simulated at temperatures of 1000 K or higher, because its

Table 7.2. *PIMC energy and reference data. All PIMC calculations are in good agreement with the reference data. Energies are in the Hartree atomic units. The footnotes are: [a] – analytical result [23, p. 88], [b] – the system is dissociated at this temperature.*

$E(E_\mathrm{h})$	T	H (AQ)	H (BO)	^{4}He (AQ)	He (BO)
	300 K	$-0.49975(12)$	$-0.49996(8)$	$-2.9027(14)$	$-2.9030(9)$
PIMC	1000 K	$-0.49979(13)$	$-0.49995(8)$	$-2.9020(20)$	$-2.9040(15)$
	3000 K	$-0.49976(16)$	$-0.50008(15)$	$-2.9019(21)$	$-2.9023(9)$
Ref.	0 K	-0.49973 [a]	-0.5 [a]	-2.9033 [24]	-2.9037 [25]

$E(E_\mathrm{h})$	T	H_2	HD	D_2	H_2 (BO$_{r=1.4\,a_0}$)
	300 K	$-1.1641(6)$	$-1.1646(12)$	$-1.1660(6)$	$-1.1753(24)$
PIMC	1000 K	$-1.1618(8)$	$-1.1624(13)$	$-1.1633(8)$	$-1.1763(25)$
	3000 K	$-1.1508(8)$	$-1.1520(16)$	$-1.1526(9)$	$-1.1755(28)$
Ref.	0 K	-1.1640 [26]	-1.1655 [27]	-1.1672 [28, 27]	-1.1745 [29]

$E(E_\mathrm{h})$	T	Ps	Ps_2	H_2^+
	100 K	$-0.249977(21)$	$-0.51589(15)$	
	300 K	$-0.24997(4)$	$-0.51594(15)$	$-0.5971(10)$
PIMC	500 K		$-0.51595(16)$	
	1000 K	$-0.24999(4)$	[b]	$-0.5943(14)$
	3000 K	$-0.24997(4)$		[b]
Ref.	0 K	-0.25 [a]	-0.51600 [30]	-0.5971 [31]

ground state $-0.516\,E_\mathrm{h}$ is near the dissociated state $2E_\mathrm{Ps} = -0.50\,E_\mathrm{h}$. Dipositronium is calculated at additional temperatures 100 K and 500 K, so that temperature dependence can be inspected. The energy of dipositronium is not temperature dependent, unlike other diatomic AQ molecules.

7.4 Diamagnetic susceptibility

In this section we present the diamagnetic suspectibilities based on PIMC simulations, and compare the results to selected 0 kelvin references values. The references values [6, 27, 28, 30, 32–44] are based on various methods and do not fully agree with each other or the results from PIMC. Some systems do not have a reference value for the diamagnetic suspectibility, to the best of our knowledge.

A method developed by Rebane [32] is used to calculate some reference values. This method can be used to estimate the diamagnetic susceptibilities of AQ/BO systems that are charge neutral and contain only two kinds of particles. The method is based on the mean distances between pairs of particles, which are easily obtained from the literature. However, the method does not seem to be accurate for nonadiabatic many-nuclei systems. Despite uncertainty of the accuracy, calculated values of this method are still

included to the set of references values.

7.4.1 Monatomic systems

The susceptibilities of monatomic systems H and He are presented in table 7.3 and plotted in figure 7.2. The hydrogen atom shows a clear distinction between AQ and BO calculations, because the adiabatic coupling has a notable effect on the susceptibility. The effect cannot be distinguished from the helium atom, because its nucleus is much heavier, which is closer to the BO nucleus. Both the hydrogen and the helium are invariant to the temperature, because the single nucleus does not have any rotational or vibrational states.

Table 7.3. *Diamagnetic susceptibilities of monatomic systems from PIMC and selected references [32–38]. The susceptibilities are in units of* $-10^{-11}\ \frac{m^3}{mol}$ *.*

χ	T	H (AQ)	H (BO)	^{4}He (AQ)	He (BO)
PIMC	300 K	2.989(5)	2.9861(11)	2.376(10)	2.376(10)
	1000 K	2.992(4)	2.9858(11)	2.369(17)	2.373(9)
	3000 K	2.9915(32)	2.9846(21)	2.375(8)	2.371(4)
Ref.	0 K [a]	2.99071 [b]	2.98583 [b]	2.37600 [32]	2.37569 [33]
	0 K		2.98577 [34]	2.36 [c] [35]	2.375 [36]
				2.40 [c] [37]	
				2.54(10) [c] [38]	

[a] Calculated with Rebane's method. Pair distance data is taken from indicated source.

[b] Pair distance for Rebane's method is taken from analytical equation B.14.

[c] Experimental result, $T = 298\,\mathrm{K}$.

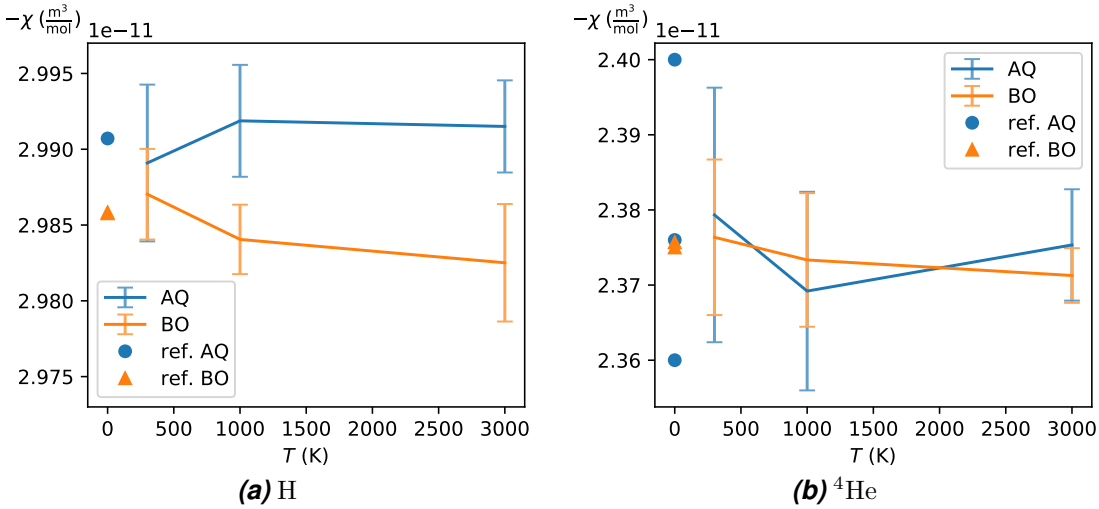

(a) H ***(b)*** $^4\mathrm{He}$

Figure 7.2. *Diamagnetic susceptibility of* H *and* He *as a function of temperature. The PIMC values at each temperature are statistically indistinguishable, and no temperature dependence is observed nor expected for these systems. Solid lines are drawn to guide the eye. The reference values are from table 7.3.*

7.4.2 Diatomic systems

Susceptibilities of diatomic systems H_2, HD, D_2 and H_2^+ are presented in tables 7.4 and 7.5. The susceptibilities of these systems increase with temperature, because the mean nuclear separation also increases due to centrifugal distortion caused by activating rotational states. The longer separation of the nuclei brings the system closer to the limit of two isolated atoms. The susceptibilities of each molecule are lower than twice the atomic susceptibilities, indicating that the bonding lowers the total susceptibility. Susceptibility of hydrogen molecule H_2 is plotted in figure 7.3a. Note that PIMC results have lower margin of error than discrepancy of 0 K AQ references. The difference between 0 K

Table 7.4. *Diamagnetic susceptibilities of diatomic systems. The susceptibilities are in units of* $-10^{-11}\ \frac{m^3}{mol}$ *.*

χ	T	H_2	HD	D_2	H_2 (BO$_{r=1.4\,a_0}$)
PIMC	300 K	5.063(24)	5.05(5)	5.039(28)	4.965(27)
	1000 K	5.075(19)	5.084(34)	5.082(27)	4.957(15)
	3000 K	5.200(13)	5.174(28)	5.196(29)	4.969(12)
Ref.	0 K [a]	5.2065 [27]		5.16429 [28]	5.0699 [39]
	0 K	5.1131 [42]		5.0650 [42]	5.0530 [b] [40]
	0 K	5.08 [41]			4.952 [b] [42]
	0 K	5.04 [c] [44, p. 812]			4.815 [b] [43]
	0 K	5.01 [c] [44, p. 812]			
	300 K	5.080(3) [6]			

[a] Calculated with Rebane's method. Pair distance data is taken from indicated source.

[b] Isotropic susceptibility is obtained by calculating rotational average.

[c] Experimental value, temperature not available.

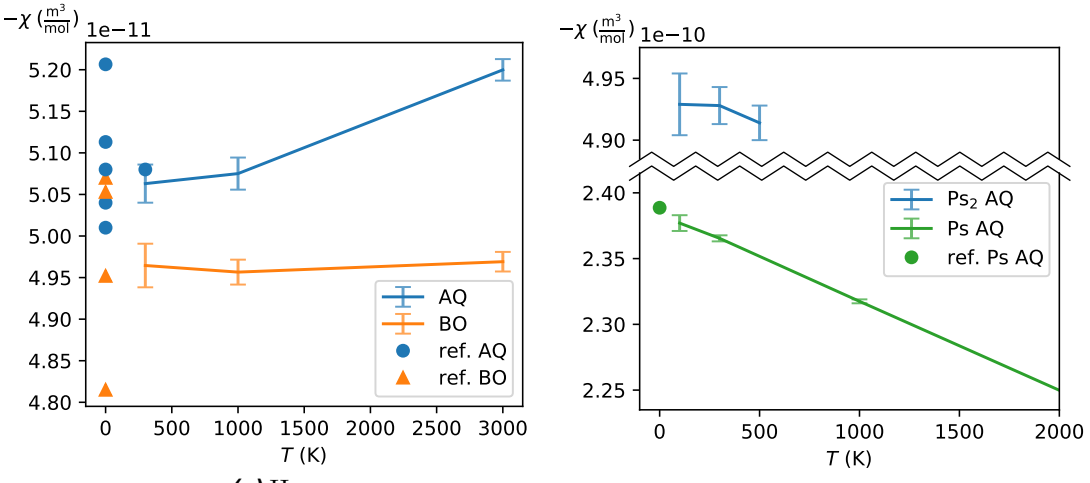

(a) H_2 ***(b)*** Ps *and* Ps_2

Figure 7.3. *Diamagnetic susceptibility of* H_2, Ps *and* Ps_2 *at various temperatures along with reference values [6, 27, 32, 39–41, 43, 44] from tables 7.4 and 7.5.*

AQ and BO values is caused by the zero-point vibration.

7.4.3 Systems with low nuclear mass

Susceptibilities of exotic systems Ps and Ps_2 are presented in table 7.5 and plotted in figure 7.3b. The susceptibility of positronium decreases at higher temperatures, unlike the rest of the monoatomic systems, which did not show notable thermal effects. Again, the susceptibility of dipositronium shows no statistically meaningful decrease with the temperature. Note that unlike H_2, the susceptibility of Ps_2 is greater than the susceptibility of two separate positroniums. For this reason, the susceptibility of Ps_2 is expected to decrease at higher temperatures. Result of dipositronium differs considerably from Rebane's reference value, which is not a large concern, as Rebane's method has unclear precision for systems with multiple nuclei. The susceptibilities of Ps and Ps_2 have not been studied at finite temperatures before.

Last, the effect of nuclear mass is inspected on diatomic molecules. Figure 7.4 presents the susceptibilities of numerous artificial hydrogen-like molecules, which vary the nuclear mass on range from positron to eight times mass of a proton. The figure shows a smooth transition from dipositronium to the hydrogen molecule and beyond. An approximate shape of the data is presented by fitting a curve $\chi = am^{-1} + bm^{-\frac{1}{2}} + cm^{-\frac{1}{3}} + \chi_{\mathrm{BO}}$. This curve is only an approximation, and it is not a model reflecting the physical phenomenon. Concerning the temperature $T = 1000\,\mathrm{K}$ and nuclear mass $m \geq 3m_{\mathrm{e}}$, the coefficients are $a = -1.62 \times 10^{-13} \frac{\mathrm{m}^3}{\mathrm{mol}\,\mathrm{m_p}}$, $b = 1.20 \times 10^{-12} \frac{\mathrm{m}^3}{\mathrm{mol}\sqrt{\mathrm{m_p}}}$ and $c = -2.83 \times 10^{-12} \frac{\mathrm{m}^3}{\mathrm{mol}\sqrt[3]{\mathrm{m_p}}}$. The error of the fit is less than 1% for each data point.

Table 7.5. *Diamagnetic susceptibilities. The susceptibilities are in units of* $-10^{-11}\,\frac{m^3}{mol}$ *.*

χ	T	Ps	Ps_2	H_2^+
	100 K	$23.77(6)$	$49.29(25)$	
	300 K	$23.654(23)$	$49.28(15)$	$2.318(28)$
PIMC	500 K		$49.14(14)$	
	1000 K	$23.175(16)$	[d]	$2.331(23)$
	3000 K	$21.822(14)$		[d]
Ref.	0 K	23.88663 [a b]	69.7449 [a] [30]	2.37944 [c] [45]

[a] Calculated with Rebane's method. Pair distance data is taken from indicated source.

[b] Using analytical pair distance from equation B.14.

[c] BO calculation. Isotropic susceptibility is obtained by calculating rotational average.

[d] Nuclei are dissociated at this temperature.

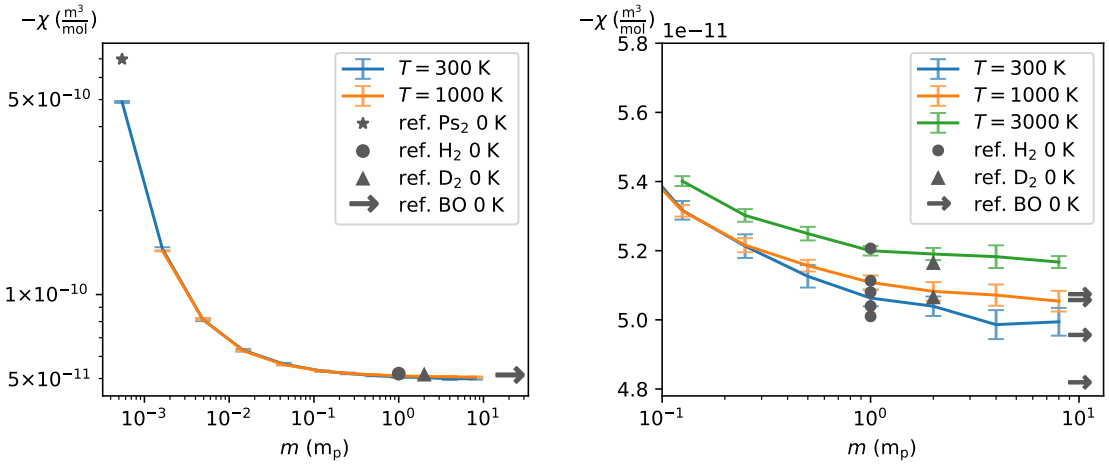

(a) *Nucleus masses from m_e to $8m_\mathrm{p}$* ***(b)*** *Nucleus masses from $\frac{m_\mathrm{p}}{8}$ to $8m_\mathrm{p}$*

Figure 7.4. *Diamagnetic susceptibilities of hydrogen-like diatomic molecules, whose nuclear masses have been varied. The horizontal axis value $m = 1\,m_\mathrm{p}$ corresponds to the hydrogen molecule, $m = 2\,m_\mathrm{p}$ corresponds to the deuterium molecule, and $m = \frac{1}{1836}\,m_\mathrm{p}$ corresponds to the dipositronium. Figure (b) is a smaller section of figure (a). The reference values are the same as in table 7.4.*

7.5 Correlation considerations

Susceptibilities of Ps and Ps_2 are an order of magnitude higher than for other systems. This can be explained with the imaginary-time trajectories of the particles. The trajectories of each particle are spread out according to their thermal wave length, which is proportional to $\frac{1}{\sqrt{mT}}$. In case of the hydrogen atom, the trajectory of the nucleus is almost point-like compared to the large trajectory of the electron. However, in case of the positronium, the trajectory of nucleus has a size equal to the trajectory of the electron. The longer thermal wave length leads to an increased extent of the particle trajectory, which increases trajectory area, affecting the susceptibility.

The temperature-dependencies of Ps and Ps_2 are interesting, as it shows that the temperatures can couple directly with the electronic structure if the nucleus is light enough. One possible explanation is that as the temperature rises, the imaginary-time trajectories shrink, but the mean particle distances remain constant. This causes the particle trajectories to have less overlap between each other. The PIMC calculation of positronium shows that at 3000 K the positron is spread out on a scale that is comparable to interparticle distance ($\approx 3\,a_0$), but at 300 K the spread is an order of magnitude larger.

The susceptibility depends strongly on the correlation of the trajectories. This can be demonstrated with a system consisting of two particles that are denoted with a and b. The susceptibility in equation 5.12 can be decomposed as

$$\chi \propto \left\langle (q_a \mathcal{A}_a + q_b \mathcal{A}_b)^2 \right\rangle \tag{7.5}$$

$$= q_a^2 \left\langle \mathcal{A}_a^2 \right\rangle + q_b^2 \left\langle \mathcal{A}_b^2 \right\rangle + 2 q_a q_b \left\langle \mathcal{A}_a \mathcal{A}_b \right\rangle \tag{7.6}$$

where q is the charge and $\mathcal{A}$ is the area of the trajectory. Examples of two-electron systems are the positronium and the BO hydrogen molecule. In case of the positronium, $q_a q_b < 0$, and so the correlation term $\langle \mathcal{A}_a \mathcal{A}_b \rangle$ decreases susceptibility. In case of the BO hydrogen molecule, $q_a q_b > 0$, and so the correlation term increases susceptibility. However, there is no easy way to reason terms $\langle \mathcal{A}_a^2 \rangle$, $\langle \mathcal{A}_b^2 \rangle$ and $\langle \mathcal{A}_a \mathcal{A}_b \rangle$ intuitively. For example, it may appear intuitive, that shorter bond length of H_2 increases the electron overlap, which would then increase the correlation term $\langle \mathcal{A}_a \mathcal{A}_b \rangle$. However, the correlation term of H_2 is actually not affected, and the change in susceptibility is caused by terms $\langle \mathcal{A}_a^2 \rangle$ and $\langle \mathcal{A}_b^2 \rangle$. On the other hand, positronium shows strong changes in all three terms when the temperature is changed, which may be unexpected. So, the temperature dependency of the susceptibility depends on both the correlation and the thermal wavelength of the particle trajectories.

8 CONCLUSION

In this work we cover-imaginary time Feynman path integrals for distinguishable quantum mechanical particles, and we derive an estimator of diamagnetic susceptibility for the PIMC method. Even though the estimator has been presented before [20], the derivation in this work is new and well detailed. The estimator is applied in simulations of molecules, and the produced results are compared to reference values, which shows that the estimator is accurate.

The PIMC method has a rare capability to simulate fully nonadiabatic systems at finite temperatures, which is beyond reach for most methods. This makes PIMC a suitable tool for finding exact quantum mechanical properties at finite temperatures. However, there still exists a major challenge: If the system is larger than a few particles, the computational demand grows steeply. To obtain the best statistical accuracy, this work considers only small systems at relatively high temperatures.

The diamagnetic susceptibility is calculated for light atoms and molecules. The results show clear effects due to nonadiabatic coupling between electrons and nuclei, which is about 0.2% for the hydrogen atom and about 2% for the hydrogen molecule. This highlights the importance of nonadiabatic calculations with light nuclei. Diatomic molecules show clear temperature dependencies, which creates a difference of about 3% on a temperature range 300–$3000\,\mathrm{K}$. This highlights that the finite temperature should be accounted with multinuclear systems. Exotic positronium systems show unexpected temperature dependencies, which suggests that the temperature couples with electronic structure if the nucleus is very light.

It is worth emphasizing that the presented results bring up new information that has not been calculated before. Namely, there is little to no previous calculations on diamagnetic susceptibility at finite temperatures. Also, there is no precise consensus on nonadiabatic $0\,\mathrm{K}$ reference values either, and presented results on hydrogen molecule have lower margins of error than the discrepancy between the nonadiabatic reference values.

One has to keep in mind that presented results cover only the diamagnetic susceptibility in the zero-field limit, so realistic situations should also consider effects including the paramagnetic contribution and the finite magnetic field. For reference, the paramagnetic contribution of hydrogen molecule is about 2% [6] of the total susceptibility. On the other hand, the assumption of zero magnetic field does not pose an error in susceptibility for most diamagnetic materials, even if the magnetic field strengths are as high as in appli-

cations of NMR and MRI [7, p. 65].

The NMR and MRI applications require accuracy of susceptibility that is preferably of the order of 0.1% or smaller [7, p. 68]. Because the presented diamagnetic susceptibilities have accuracies varying on range 0.1–1%, they may be useful for these applications, if the paramagnetic contribution can be accounted by other means.

Even though the PIMC is currently practical only with small molecules, larger systems will become available in the future, as the algorithmical efficiency improves and the computational resources grow. Due to its exact nature in finite temperatures, the PIMC has a great potential to become a more widely used quantum simulation method for the magnetic properties.

REFERENCES

[1] Ceperley, D. Path Integrals in the Theory of Condensed Helium. *Reviews of Modern Physics* 67.2 (Apr. 1, 1995), 279–355. ISSN: 0034-6861, 1539-0756. DOI: 10.1103/RevModPhys.67.279. URL: https://link.aps.org/doi/10.1103/RevModPhys.67.279 (visited on 12/20/2017).

[2] Kylänpää, I. *First-Principles Finite Temperature Electronic Structure of Some Small Molecules*. PhD Thesis. Tampere University of Technology, Nov. 1, 2011. ISBN: 978-952-15-2662-6. URL: https://trepo.tuni.fi/handle/10024/114461.

[3] Tiihonen, J. Thermal Effects in Atomic and Molecular Polarizabilities with Path Integral Monte Carlo. (Apr. 5, 2019), 188. URL: https://trepo.tuni.fi/handle/10024/113903.

[4] Vaara, J. Theory and Computation of Nuclear Magnetic Resonance Parameters. *Physical Chemistry Chemical Physics* 9.40 (2007), 5399. ISSN: 1463-9076, 1463-9084. DOI: 10.1039/b706135h. URL: http://xlink.rsc.org/?DOI=b706135h (visited on 04/01/2021).

[5] Ruud, K., Vaara, J., Lounila, J. and Helgaker, T. Vibrationally Averaged Magnetizabilities and Rotational g Tensors of the Water Molecule. *Chemical Physics Letters* 297.5-6 (Dec. 1998), 467–474. ISSN: 00092614. DOI: 10.1016/S0009-2614(98)01155-5. URL: https://linkinghub.elsevier.com/retrieve/pii/S0009261498011555 (visited on 02/03/2021).

[6] Ruud, K., Åstrand, P.-O., Helgaker, T. and Mikkelsen, K. V. Full CI Calculations of the Magnetizability and Rotational g Factor of the Hydrogen Molecule. *Journal of Molecular Structure: THEOCHEM* 388 (Dec. 1996), 231–235. ISSN: 01661280. DOI: 10.1016/S0166-1280(96)80036-4. URL: https://linkinghub.elsevier.com/retrieve/pii/S0166128096800364 (visited on 01/30/2021).

[7] Harris, R. K., Becker, E. D., Cabral de Menezes, S. M., Granger, P., Hoffman, R. E. and Zilm, K. W. Further Conventions for NMR Shielding and Chemical Shifts (IUPAC Recommendations 2008). *Pure and Applied Chemistry* 80.1 (Jan. 1, 2008), 59–84. ISSN: 1365-3075, 0033-4545. DOI: 10.1351/pac200880010059. URL: https://www.degruyter.com/document/doi/10.1351/pac200880010059/html (visited on 03/06/2021).

[8] Feynman, R., Hibbs, A. and Styer, D. *Quantum Mechanics and Path Integrals*. Dover Books on Physics. Dover Publications, 2010. ISBN: 978-0-486-47722-0. URL: https://books.google.fi/books?id=JkMuDAAAQBAJ.

[9] Seahra, S. S. Path Integrals in Quantum Field Theory. (May 11, 2000), 36.

[10] Feynman, R. Space-Time Approach to Non-Relativistic Quantum Mechanics. 20 (1948), 367–387. DOI: 10.1103/RevModPhys.20.367.

[11] Kleinert, H. *Path Integrals in Quantum Mechanics, Statistics, and Polymer Physics*. WORLD SCIENTIFIC, Sept. 1990. ISBN: 978-981-02-0196-8. DOI: 10.1142/1081. URL: https://www.worldscientific.com/worldscibooks/10.1142/1081 (visited on 06/21/2020).

[12] Grosche, C. *An Introduction into the Feynman Path Integral*. Feb. 20, 1993. arXiv: hep-th/9302097. URL: http://arxiv.org/abs/hep-th/9302097 (visited on 04/24/2021).

[13] Gaveau, B., Mihokova, E., Roncadelli, M. and Schulman, L. S. Path Integral in a Magnetic Field Using the Trotter Product Formula. *American Journal of Physics* 72.3 (Mar. 2004), 385–388. ISSN: 0002-9505, 1943-2909. DOI: 10.1119/1.1630334. arXiv: quant-ph/0403019. URL: http://arxiv.org/abs/quant-ph/0403019 (visited on 09/04/2019).

[14] Boyer, T. H. Darwin-Lagrangian Analysis for the Interaction of a Point Charge and a Magnet: Considerations Related to the Controversy Regarding the Aharonov-Bohm and Aharonov-Casher Phase Shifts. *Journal of Physics A: Mathematical and General* 39.13 (Mar. 31, 2006), 3455–3477. ISSN: 0305-4470, 1361-6447. DOI: 10.1088/0305-4470/39/13/021. arXiv: physics/0506181. URL: http://arxiv.org/abs/physics/0506181 (visited on 10/07/2020).

[15] Kdziera, D., Stanke, M., Bubin, S., Barysz, M. and Adamowicz, L. Darwin and Mass-Velocity Relativistic Corrections in the Non-Born-Oppenheimer Calculations of Pure Vibrational States of H2. *The Journal of Chemical Physics* 125.1 (July 7, 2006), 014318. ISSN: 0021-9606, 1089-7690. DOI: 10.1063/1.2209691. URL: http://aip.scitation.org/doi/10.1063/1.2209691 (visited on 07/23/2020).

[16] Styer, D. *Kernel for Charged Particle in Magnetic Field: Feynman-Hibbs Problem 3-10*. Nov. 18, 2006.

[17] Shumway, J. and Ceperley, D. M. Path Integral Monte Carlo Simulations for Fermion Systems : Pairing in the Electron-Hole Plasma. *Le Journal de Physique IV* 10 (PR5 Mar. 2000), Pr5-3-Pr5–16. ISSN: 1155-4339. DOI: 10.1051/jp4:2000501. URL: http://www.edpsciences.org/10.1051/jp4:2000501 (visited on 06/08/2018).

[18] Reichl, L. E. *A Modern Course in Statistical Physics*. 4th revised and updated edition. Weinheim: Wiley-VCH Verlag GmbH & Co. KGaA, 2016. 467 pp. ISBN: 978-3-527-69046-6.

[19] Nolting, W. and Ramakanth, A. *Quantum Theory of Magnetism*. Berlin, Heidelberg: Springer Berlin Heidelberg, 2009. ISBN: 978-3-540-85415-9. DOI: 10.1007/978-3-540-85416-6. URL: http://link.springer.com/10.1007/978-3-540-85416-6 (visited on 07/03/2020).

[20] Pollock, E. L. and Runge, K. J. Pathintegral Study of Magnetic Response: Excitonic and Biexcitonic Diamagnetism in Semiconductor Quantum Dots. *The Journal of Chemical Physics* 96.1 (Jan. 1992), 674–680. ISSN: 0021-9606, 1089-7690. DOI: 10.1063/1.462451. URL: http://aip.scitation.org/doi/10.1063/1.462451 (visited on 06/20/2019).

[21] Robert, C. P. and Casella, G. *Monte Carlo Statistical Methods*. 2nd ed. Springer Texts in Statistics. New York: Springer, 2004. 645 pp. ISBN: 978-0-387-21239-5.

[22] Kylänpää, I. Computational Physics, Lecture Slides, Week 2. Jan. 7, 2019.

[23] Atkins, P. W. and Friedman, R. *Molecular Quantum Mechanics*. 5th ed. Oxford ; New York: Oxford University Press, 2011. 537 pp. ISBN: 978-0-19-954142-3.

[24] Stanke, M., Kdziera, D., Bubin, S. and Adamowicz, L. Relativistic Corrections to the Non-Born-Oppenheimer Energies of the Lowest Singlet Rydberg States of He3 and He4. *The Journal of Chemical Physics* 126.19 (May 21, 2007), 194312. ISSN: 0021-9606, 1089-7690. DOI: 10.1063/1.2735305. URL: http://aip.scitation.org/doi/10.1063/1.2735305 (visited on 07/24/2020).

[25] Drake, G. W. F. High Precision Theory of Atomic Helium. *Physica Scripta* T83.1 (1999), 83. ISSN: 0031-8949. DOI: 10.1238/Physica.Topical.083a00083. URL: http://www.physica.org/xml/article.asp?article=t083a00083.xml (visited on 07/16/2018).

[26] Bubin, S. and Adamowicz, L. Variational Calculations of Excited States with Zero Total Angular Momentum (Vibrational Spectrum) of H2 without Use of the BornOppenheimer Approximation. *The Journal of Chemical Physics* 118.7 (Feb. 15, 2003), 3079–3082. ISSN: 0021-9606, 1089-7690. DOI: 10.1063/1.1537719. URL: http://aip.scitation.org/doi/10.1063/1.1537719 (visited on 07/04/2018).

[27] Alexander, S. A. and Coldwell, R. L. Fully Nonadiabatic Properties of All H2 Isotopomers. *The Journal of Chemical Physics* 129.11 (Sept. 21, 2008), 114306. ISSN: 0021-9606, 1089-7690. DOI: 10.1063/1.2978172. URL: http://aip.scitation.org/doi/10.1063/1.2978172 (visited on 09/16/2020).

[28] Bubin, S., Stanke, M., Molski, M. and Adamowicz, L. Accurate Non-BornOppenheimer Calculations of the Lowest Vibrational Energies of D2 and T2 with Including Relativistic Corrections. *Chemical Physics Letters* 494.1-3 (July 2010), 21–25. ISSN: 00092614. DOI: 10.1016/j.cplett.2010.05.081. URL: https://linkinghub.elsevier.com/retrieve/pii/S0009261410007554 (visited on 08/23/2020).

[29] Wolniewicz, L. Nonadiabatic Energies of the Ground State of the Hydrogen Molecule. *The Journal of Chemical Physics* 103.5 (Aug. 1995), 1792–1799. ISSN: 0021-9606, 1089-7690. DOI: 10.1063/1.469753. URL: http://aip.scitation.org/doi/10.1063/1.469753 (visited on 07/04/2018).

[30] Bubin, S., Stanke, M., Kdziera, D. and Adamowicz, L. Relativistic Corrections to the Ground-State Energy of the Positronium Molecule. *Physical Review A* 75.6 (June 11, 2007). ISSN: 1050-2947, 1094-1622. DOI: 10.1103/PhysRevA.75.062504. URL: https://link.aps.org/doi/10.1103/PhysRevA.75.062504 (visited on 08/23/2020).

[31] Hijikata, Y., Nakashima, H. and Nakatsuji, H. Solving Non-BornOppenheimer Schrödinger Equation for Hydrogen Molecular Ion and Its Isotopomers Using the Free Complement Method. *The Journal of Chemical Physics* 130.2 (Jan. 14, 2009), 024102. ISSN: 0021-9606, 1089-7690. DOI: 10.1063/1.3048986. URL: http://aip.scitation.org/doi/10.1063/1.3048986 (visited on 07/23/2020).

[32] Rebane, T. K. Nonadiabatic Theory of Diamagnetic Susceptibility of Molecules. *Optics and Spectroscopy* 93.2 (Aug. 2002), 236–241. ISSN: 0030-400X, 1562-6911. DOI: 10.1134/1.1503752. URL: http://link.springer.com/10.1134/1.1503752 (visited on 07/21/2020).

[33] Haftel, M. I. and Mandelzweig, V. B. Precise Nonvariational Calculations on the Helium Atom. *Physical Review A* 38.12 (Dec. 1, 1988), 5995–5999. ISSN: 0556-2791. DOI: 10.1103/PhysRevA.38.5995. URL: https://link.aps.org/doi/10.1103/PhysRevA.38.5995 (visited on 08/23/2020).

[34] Mendelsohn, L. B., Biggs, F. and Mann, J. B. Hartree-Fock Diamagnetic Susceptibilities. *Physical Review A* 2.4 (Oct. 1, 1970), 1130–1134. ISSN: 0556-2791. DOI: 10.1103/PhysRevA.2.1130. URL: https://link.aps.org/doi/10.1103/PhysRevA.2.1130 (visited on 07/10/2019).

[35] Wills, A. P. and Hector, L. G. The Magnetic Susceptibility of Oxygen, Hydrogen and Helium. *Physical Review* 23.2 (Feb. 1, 1924), 209–220. ISSN: 0031-899X. DOI: 10.1103/PhysRev.23.209. URL: https://link.aps.org/doi/10.1103/PhysRev.23.209 (visited on 02/12/2021).

[36] Bruch, L. W. and Weinhold, F. Diamagnetism of Helium. *The Journal of Chemical Physics* 113.19 (Nov. 15, 2000), 8667–8670. ISSN: 0021-9606, 1089-7690. DOI: 10.1063/1.1318766. URL: http://aip.scitation.org/doi/10.1063/1.1318766 (visited on 09/26/2020).

[37] Havens, G. G. The Magnetic Susceptibilities of Some Common Gases. *Physical Review* 43.12 (June 15, 1933), 992–1000. ISSN: 0031-899X. DOI: 10.1103/PhysRev.43.992. URL: https://link.aps.org/doi/10.1103/PhysRev.43.992 (visited on 02/12/2021).

[38] Barter, C., Meisenheimer, R. G. and Stevenson, D. P. Diamagnetic Susceptibilities of Simple Hydrocarbons and Volatile Hydrides. *The Journal of Physical Chemistry* 64.9 (Sept. 1960), 1312–1316. ISSN: 0022-3654, 1541-5740. DOI: 10.1021/j100838a045. URL: https://pubs.acs.org/doi/abs/10.1021/j100838a045 (visited on 09/26/2020).

[39] Alexander, S. A. and Coldwell, R. L. Rovibrationally Averaged Properties of H2 Using Monte Carlo Methods. *International Journal of Quantum Chemistry* 107.2 (2007), 345–352. ISSN: 00207608, 1097461X. DOI: 10.1002/qua.21130. URL: http://doi.wiley.com/10.1002/qua.21130 (visited on 09/16/2020).

[40] Alijah, A., Vieyra, J. C. L., Nader, D. J., Turbiner, A. V. and Cobaxin, H. M. *The Hydrogen Molecule H2 in Inclined Configuration in a Weak Magnetic Field*. May 14, 2019. DOI: 10.1016/j.jqsrt.2019.05.010. arXiv: 1903.08324 [physics, physics:quant-ph]. URL: http://arxiv.org/abs/1903.08324 (visited on 09/06/2020).

[41] Glick, R. E. On the Diamagnetic Susceptibility of Gases. *The Journal of Physical Chemistry* 65.9 (Sept. 1961), 1552–1555. ISSN: 0022-3654, 1541-5740. DOI: 10.1021/j100905a020. URL: http://pubs.acs.org/doi/abs/10.1021/j100905a020 (visited on 06/27/2019).

[42] Ishiguro, E. and Koide, S. Magnetic Properties of the Hydrogen Molecules. *Physical Review* 94.2 (Apr. 15, 1954), 350–357. ISSN: 0031-899X. DOI: 10.1103/PhysRev.94.350. URL: https://link.aps.org/doi/10.1103/PhysRev.94.350 (visited on 09/28/2020).

[43] Raynes, W. T., Riley, J. P., Davies, A. M. and Cook, D. B. A Note on the Magnetic Susceptiblllty. 24.1 (1974), 5.

[44] M. Jain and R. R. Gupta, eds. *Diamagnetic Susceptibility and Anisotropy of Inorganic and Organometallic Compounds*. Berlin: Springer, 2007. 387 pp. ISBN: 978-3-540-23113-4.

[45] Cobaxin, H. M., Alijah, A., Vieyra, J. C. L. and Turbiner, A. V. $\mathrm H_2ˆ+$ in a Weak Magnetic Field. *Journal of Physics B: Atomic, Molecular and Optical Physics* 48.4 (Feb. 28, 2015), 045101. ISSN: 0953-4075, 1361-6455. DOI: 10.1088/0953-4075/48/4/045101. arXiv: 1409.6204. URL: http://arxiv.org/abs/1409.6204 (visited on 10/04/2019).

[46] Tokmakoff, A. *5.74 Introductory Quantum Mechanics II, Linear Response Theory*. 2009. URL: https://ocw.mit.edu/courses/chemistry/5-74-introductory-quantum-mechanics-ii-spring-2009/lecture-notes/MIT5_74s09_lec07.pdf.

[47] Hofmann, P. *Solid State Physics: An Introduction*. Second edition. Weinheim: Wiley-VCH, Verlag GmbH & Co. KGaA, 2015. 248 pp. ISBN: 978-3-527-41282-2.

[48] Tolvanen, A. *Simulation Data in This Thesis. Replication Templates and Supplementary Results.* URL: https://gitlab.com/tolvanea/msc-thesis.

[49] *Electronic Structure Theory, Theoretical and Computational Materials Physics*. URL: https://research.tuni.fi/est/.

A DYNAMIC SUSCEPTIBILITY

The dynamic susceptibility is derived for a time-dependent system by using the operator formalism. The system is at zero temperature.

A.1 Linear response theory

Let H_0 be a time-independent Hamiltonian of a homogenic system in equilibrium. An external time-dependent perturbation $\hat{H}_{\text{ext}}(t)$ is turned on at time $t = 0$ so that $\hat{H}_{\text{ext}}(t) = 0$ if $t < 0$. A total Hamiltonian is then

$$\hat{H}(t) = \hat{H}_0 + \hat{H}_{\text{ext}}(t). \tag{A.1}$$

The perturbation is formed by some external field $F(t)$ interacting to an internal variable, which has an observable $\hat{Q}$. The perturbation is

$$\hat{H}_{\text{ext}}(t) = -F(t)\hat{Q}, \tag{A.2}$$

where $F(t) = 0$ if $t < 0$. For example, $F(t)$ can be a strength of the electric field in x-direction and $\hat{Q}$ can be the electric polarization operator in the same direction. Alternatively, $F(t)$ and $\hat{Q}$ can correspond to the magnetic field and the magnetic moment operator respectively. This is similar to the section 4. Note that both $F(t)$ and $\left\langle \hat{Q} \right\rangle$ are real valued quantities.

At $t < 0$ the system is in the equilibrium, i.e. $\left\langle \hat{Q} \right\rangle (t) = \left\langle \hat{Q} \right\rangle_{\hat{H}_0}$. The time dependence of $\left\langle \hat{Q} \right\rangle (t)$ can be expanded with series [46]

$$\left\langle \hat{Q} \right\rangle (t) = \left(\text{terms } F^{(0)}\right) + \left(\text{terms } F^{(1)}\right) + \cdots \tag{A.3}$$

$$= \left\langle \hat{Q} \right\rangle_{\hat{H}_0} + \delta \left\langle \hat{Q} \right\rangle (t) + \cdots \tag{A.4}$$

where $\delta \left\langle \hat{Q} \right\rangle (t)$ denotes a linear response term. If the perturbation is small, the linear response is enough to describe the system. It is

$$\delta \left\langle \hat{Q} \right\rangle (t) = \int_0^\infty \mathrm{d}t' \chi(t') F(t - t'), \tag{A.5}$$

where $\mathrm{d}t'$ integrates all times backwards in history, and $\chi(t')$ is a linear response function,

which determines how much past values of $F(t-t')$ affect the current value of $\left\langle \hat{Q} \right\rangle (t)$. For example, if the magnetic field is suddenly applied to the material, the material takes some time to fully magnetize, and the response function determines that memory effect. It can be easily shown that the linear response function $\chi(t')$ is an impulse response, that is, if $F(t-t')$ is replaced with the Dirac delta function $\delta(t-t')$, then

$$\int_0^\infty \mathrm{d}t' \chi(t') \delta(t-t') = \chi(t), \tag{A.6}$$

meaning that $\delta \left\langle \hat{Q} \right\rangle (t) = \chi(t)$ for the impulse $F(t) = \delta(t)$. It is also evident that $\chi(t)$ is a real function.

By defining that $\chi(t') = 0$ when $t' < 0$, the equation A.5 can be written without the lower integration bound

$$\delta \left\langle \hat{Q} \right\rangle (t) = \int_{-\infty}^\infty \mathrm{d}t' \chi(t') F(t-t'). \tag{A.7}$$

This definition of χ is useful, because the equation A.7 can be expressed with a *convolution* of χ and F. The convolution of two functions $f(t)$ and $g(t)$ is defined as

$$(f * g)(t) \equiv \int_{-\infty}^\infty \mathrm{d}t' f(t') g(t-t'). \tag{A.8}$$

A fourier transform of the convolution has a simple expression

$$\widetilde{(f * g)}(\omega) = \widetilde{f}(\omega) \widetilde{g}(\omega), \tag{A.9}$$

where the Fourier transform is defined as

$$\widetilde{f}(\omega) = \int_{-\infty}^\infty \mathrm{d}t f(t) e^{-\mathrm{i}\omega t} \tag{A.10}$$

$$\widetilde{f}(t) = \frac{1}{2\pi} \int_{-\infty}^\infty \mathrm{d}\omega \widetilde{f}(\omega) e^{\mathrm{i}\omega t}. \tag{A.11}$$

Therefore, the equation A.7 can be written as the convolution in frequency domain with

$$\left\langle \hat{\widetilde{Q}} \right\rangle (\omega) = \widetilde{\chi}(\omega) \widetilde{F}(\omega). \tag{A.12}$$

The response function χ is also called the *dynamic susceptibility*.

A.2 Dynamic susceptibility

This section derives a following formula for the dynamic susceptibility

$$\chi(t) = \frac{\mathrm{i}}{\hbar} \theta(t) \left\langle \left[\hat{Q}(t), \hat{Q}(0) \right] \right\rangle, \tag{A.13}$$

where $\left[\hat{A},\hat{B}\right] = \hat{A}\hat{B} - \hat{B}\hat{A}$ is the commutator, and the expectation value $\langle\cdot\rangle$ corresponds to the unperturbed system. The derivation follows loosely sources [11, p. 1262][46, p. 8-11]

The perturbed Hamiltonian $\hat{H} = \hat{H}_0 + \hat{H}_{\text{ext}}$ from equation A.1 has the time evolution operator

$$\hat{U}(t) = e^{-\frac{\mathrm{i}}{\hbar}\int_0^t \hat{H}(t)} \tag{A.14}$$

$$= e^{-\frac{\mathrm{i}}{\hbar}\left(\hat{H}_0 t + \int_0^t \mathrm{d}t' \hat{H}_{\text{ext}}(t')\right)} \tag{A.15}$$

$$= e^{-\frac{\mathrm{i}}{\hbar}\hat{H}_0 t}\hat{U}_{\text{ext}}(t). \tag{A.16}$$

The expectation value of a Schrödinger observable $\hat{P}$ in the perturbed state is

$$\langle\phi(t)|\hat{P}|\phi(t)\rangle = \left\langle \hat{U}(t)\phi(0)\middle|\hat{P}\middle|\hat{U}(t)\phi(0)\right\rangle \tag{A.17}$$

$$= \langle\phi(0)|\hat{U}^*(t)\hat{P}\hat{U}(t)|\phi(0)\rangle \tag{A.18}$$

$$= \langle\phi(0)|\hat{U}^*_{\text{ext}}(t)\underbrace{e^{+\frac{\mathrm{i}}{\hbar}\int_0^t \mathrm{d}t' \hat{H}_0(t')}\,\hat{P}\,e^{-\frac{\mathrm{i}}{\hbar}\int_0^t \mathrm{d}t' \hat{H}_0(t')}}_{\hat{P}_{\hat{H}_0}(t)}\hat{U}_{\text{ext}}(t)|\phi(0)\rangle\,, \tag{A.19}$$

where the operator $\hat{P}_{\hat{H}_0}(t)$ measures the unperturbed system in the Heisenberg picture. In the Heisenberg picture, the time dependence has been moved from the state ϕ to the operator $\hat{P}$.

The time evolution of the perturbation can be expressed with the series [11, p. 1263]

$$\hat{U}_{\text{ext}}(t) = 1 - \frac{\mathrm{i}}{\hbar}\int_0^t \mathrm{d}t' \hat{H}_{\text{ext}}(t') + \cdots\,, \tag{A.20}$$

with which the equation A.19 becomes

$$\langle\phi(0)|\left(1 + \frac{\mathrm{i}}{\hbar}\int_0^t \mathrm{d}t' \hat{H}_{\text{ext}}(t') + \cdots\right)\hat{P}_{\hat{H}_0}(t)\left(1 - \frac{\mathrm{i}}{\hbar}\int_0^t \mathrm{d}t' \hat{H}_{\text{ext}}(t') + \cdots\right)|\phi(0)\rangle \tag{A.21}$$

$$= \langle\phi(0)|\hat{P}_{\hat{H}_0}(t)|\phi(0)\rangle \;-\; \frac{\mathrm{i}}{\hbar}\int_0^t \mathrm{d}t' \,\langle\phi(0)|\left[\hat{P}_{\hat{H}_0}(t), \hat{H}_{\text{ext}}(t')\right]|\phi(0)\rangle \;+\; \cdots\,. \tag{A.22}$$

This can be written in a more compact form

$$\left\langle\hat{P}\right\rangle(t) \approx \left\langle\hat{P}\right\rangle_{\hat{H}_0} \underbrace{-\frac{\mathrm{i}}{\hbar}\int_0^t \mathrm{d}t' \left\langle\left[\hat{P}_{\hat{H}_0}(t), \hat{H}_{\text{ext}}(t')\right]\right\rangle_{\hat{H}_0}}_{\delta\left\langle\hat{P}\right\rangle(t)} + \cdots\,, \tag{A.23}$$

where the linear term is

$$\delta\left\langle\hat{P}\right\rangle(t) = -\frac{\mathrm{i}}{\hbar}\int_0^t \mathrm{d}t' \left\langle\left[\hat{P}_{\hat{H}_0}(t), \hat{H}_{\text{ext}}(t')\right]\right\rangle_{\hat{H}_0}. \tag{A.24}$$

If the perturbation is small, higher order terms vanish, and only the linear term is left. It is worth noting that the averages correspond to the unperturbed system, so the small perturbation can be calculated without the simulation of the perturbed system.

By inserting $\hat{H}_{\mathrm{ext}}(t) = -F(t)\hat{Q}_{\hat{H}_0}(t)$ from equation A.2 to equation A.24 gives

$$\delta\left\langle \hat{P}\right\rangle(t) = -\frac{\mathrm{i}}{\hbar}\int_0^t \mathrm{d}t' \left\langle \left[\hat{P}_{\hat{H}_0}(t), -F(t')\hat{Q}_{\hat{H}_0}(t')\right]\right\rangle_{\hat{H}_0} \tag{A.25}$$

$$= \frac{\mathrm{i}}{\hbar}\int_0^t \mathrm{d}t' \left\langle \left[\hat{P}_{\hat{H}_0}(t), \hat{Q}_{\hat{H}_0}(t')\right]\right\rangle_{\hat{H}_0} F(t') \tag{A.26}$$

$$= \frac{\mathrm{i}}{\hbar}\int_0^t \mathrm{d}t'' \left\langle \left[\hat{P}_{\hat{H}_0}(t), \hat{Q}_{\hat{H}_0}(t-t'')\right]\right\rangle_{\hat{H}_0} F(t-t''), \tag{A.27}$$

where the last line applies a change of variables $t' = t - t''$. The last line also flips the integration limits reversing the integration order, which may not be apparent at the first glance. A reference point of the Heisenberg operators can be shifted from $t = 0$ to $t = -\infty$, which changes the upper integration limit of A.27 from t to ∞. Operators under the expectation value can be time-shifted by $-(t - t'')$, because the corresponding Schrödinger operators are time-independent. These manipulations result the integral in form

$$\delta\left\langle \hat{P}\right\rangle(t) = \frac{\mathrm{i}}{\hbar}\int_0^\infty \mathrm{d}t'' \left\langle \left[\hat{P}_{\hat{H}_0}(t''), \hat{Q}_{\hat{H}_0}(0)\right]\right\rangle_{\hat{H}_0} F(t-t''). \tag{A.28}$$

Last, the lower integration bound can be removed by inserting a Heaviside step function $\theta(t)$, which results

$$\delta\left\langle \hat{P}\right\rangle(t) = \frac{\mathrm{i}}{\hbar}\int_{-\infty}^\infty \mathrm{d}t''\theta(t'') \left\langle \left[\hat{P}_{\hat{H}_0}(t''), \hat{Q}_{\hat{H}_0}(0)\right]\right\rangle_{\hat{H}_0} F(t-t''). \tag{A.29}$$

If this is compared to equation A.7, the dynamic susceptibility is recognized as

$$\chi_{\hat{P}\hat{Q}}(t) = \frac{\mathrm{i}}{\hbar}\theta(t) \left\langle \left[\hat{P}_{\hat{H}_0}(t), \hat{Q}_{\hat{H}_0}(0)\right]\right\rangle_{\hat{H}_0}. \tag{A.30}$$

This equation is in more general form than equation A.13, which has assigned $\hat{Q}$ in place of the operator $\hat{P}$. That is, $\chi(t) = \chi_{\hat{Q}\hat{Q}}(t)$. For example, if F, $\hat{Q}$, and $\hat{P}$ correspond to B_x, $\hat{m}_x$ and $\hat{m}_y$ respectively, then $\chi_{\hat{m}_y\hat{m}_x}(t)$ describes how the magnetic moment $\hat{m}$ is induced in y-direction by having the magnetic field B in x-direction. This equation can be also utilized in calculation of higher order responses, such as a quadrupole response [3].

B DIAMAGNETISM OF ATOMIC HYDROGEN

An alternative representation of the static magnetic susceptibility is derived with the operator formalism. The exact diamagnetic susceptibility is calculated for the Born–Oppenheimer hydrogen atom at zero temperature.

Consider one electron system that has the nucleus fixed in origin. Shall the system be affected by the external magnetic field. The magnetic interaction is included into the Hamiltonian with a minimal substitution $\hat{\boldsymbol{p}} \to \hat{\boldsymbol{p}} - q\boldsymbol{A}(\boldsymbol{r})$, which is

$$\hat{H} = \frac{\left(\hat{\boldsymbol{p}} - q\boldsymbol{A}(\boldsymbol{r})\right)^2}{2m} + V(\boldsymbol{r}). \tag{B.1}$$

Applying a homogeneous magnetic field $\boldsymbol{B} = [0, 0, B]^T$ to equation 2.31 gives the vector potential

$$\boldsymbol{A}(x, y, z) = \frac{B}{2}\left[-y, x, 0\right]^T. \tag{B.2}$$

By utilizing properties of the Coulomb gauge, the Hamiltonian can be written [11, p. 180][19, p. 11][47, p. 162]

$$\hat{H} = \left(\frac{\hat{\boldsymbol{p}}^2}{2m} + V\right) - \frac{q}{2m}\left(\boldsymbol{r} \times \hat{\boldsymbol{p}}\right)_z B + \frac{q^2 B^2}{8m}\left(x^2 + y^2\right) \tag{B.3}$$

$$= \hat{H}_0 - \gamma \hat{\boldsymbol{L}}_z B + \frac{q^2 B^2}{8m}\left(x^2 + y^2\right), \tag{B.4}$$

where $\hat{H}_0$ is the Hamiltonian without magnetic field and $\hat{\boldsymbol{L}} = \boldsymbol{r} \times \hat{\boldsymbol{p}}$ is the angular momentum operator. The reference point of $\left(x^2 + y^2\right)$ is at the origin, where the hydrogen nucleus also lies. The Hamiltonian can be also written in form

$$\hat{H} = \hat{H}_0 - \hat{m}_z B, \tag{B.5}$$

where the magnetic moment operator in z-direction is

$$\hat{m}_z = -\frac{\partial \hat{H}}{\partial B} \tag{B.6}$$

$$= \gamma \hat{\boldsymbol{L}}_z - \frac{q^2}{4m}\left(x^2 + y^2\right) B. \tag{B.7}$$

The first term in B.7 is the permanent magnetic moment, which does not vanish at $B = 0$. The second term is the induced magnetic moment, which corresponds to diamagnetism.

At zero temperature, the system is in the ground state, and the electron has no orbital angular momentum. Also, the diamagnetism does not consider the spin angular momentum, and so the total angular momentum is considered to be zero. The equation B.7 becomes

$$\hat{m}_z = -\frac{e^2}{4m_e}\left(x^2 + y^2\right) B, \tag{B.8}$$

which has substituted $q = -e$. Equations 4.6 and 5.5 give then the magnetic susceptibility

$$\chi_z^{\mathrm{mag}} = \mu_0 \lim_{B\to 0}\left(\frac{\partial \langle \hat{m} \rangle}{\partial B}\right) \tag{B.9}$$

$$= -\mu_0 \frac{e^2}{4m_e}\left\langle x^2 + y^2 \right\rangle. \tag{B.10}$$

Because the ground state is spherically symmetric,

$$\left\langle x^2 + y^2 \right\rangle = \frac{2}{3}\left\langle r^2 \right\rangle. \tag{B.11}$$

The ground state has a radial distribution function [23, p. 88]

$$P(r) = 4a^{-3} r^2 e^{-\frac{2r}{a}}, \tag{B.12}$$

where

$$a = \frac{4\pi\varepsilon_0 \hbar^2}{\mu e^2}. \tag{B.13}$$

Here μ is either the mass of the electron m_e or the reduced mass $\frac{m_p m_e}{m_p + m_e}$, depending on whether the Born Oppenheimer approximation is used or not. The expectation value of $\left\langle r^2 \right\rangle$ can be integrated analytically to

$$\left\langle r^2 \right\rangle = \int_0^\infty P(r) r^2 \mathrm{d}r = 3a^2. \tag{B.14}$$

Because the Born Oppenheimer approximation was assumed earlier, $\mu = m_e$, and a is Bohr radius a_0. Inserting the equations B.14 and B.11 to B.10 yields an analytical form

$$\chi^{\mathrm{mag}} = -\frac{\mu_0 e^2}{4m_e} 2a_0^2 \tag{B.15}$$

$$= -\frac{\mu_0 e^2}{2m_e} a_0^2. \tag{B.16}$$

The numerical value per mole is

$$\chi_{\mathrm{mol}}^{\mathrm{mag}} = \chi^{\mathrm{mag}} N_A \tag{B.17}$$

$$\approx -2.9858 \cdot 10^{-11}\ \frac{\mathrm{m}^3}{\mathrm{mol}}, \tag{B.18}$$

where N_A is the Avogardo constant $\approx 6.022 \times 10^{23}\ \frac{1}{\mathrm{mol}}$.

C SUPPLEMENTARY INFORMATION

The simulation results and the simulation parameters are accessible in more details via an online repository [48]. This repository contains

- more observables from the simulations, such as
  - non-extrapolated data points with the finite $\Delta\tau$,
  - pair distances of the particles $\left\langle r_{i,j} \right\rangle$, $\left\langle r_{i,j}^2 \right\rangle$, and $\left\langle r_{i,j}^{-1} \right\rangle$,
  - pair correlation distributions $P(r_{i,j})$
  - the susceptibilities for each particle individually, that is, terms proportional to the square area of the single particle $\left\langle \mathcal{A}^2 \right\rangle$,
  - cross terms between the coordinate component of the area $\langle \mathcal{A}_x \mathcal{A}_y \rangle$, which is statistically zero for all the systems, and
  - Monte Carlo walker data from the equilibrium convergence,
- more figures from the simulations,
- parameters and templates that can be used to replicate all the results,
- scripts that apply unit conversions to calculate the reference values,
- automation and data analysis code written in Python, totaling over 7000 lines of code, and
- LaTeX source code of this thesis.

The simulations are made with Fortran-based `pimc3` program, developed in our research group. The program is not yet published, so please contact us [3, 49] for the access. We are grateful for IT Center of Science Ltd. (CSC) for providing computation resources via their high-performance clusters.